Chapter III
Nematogenic Coumarin derivatives

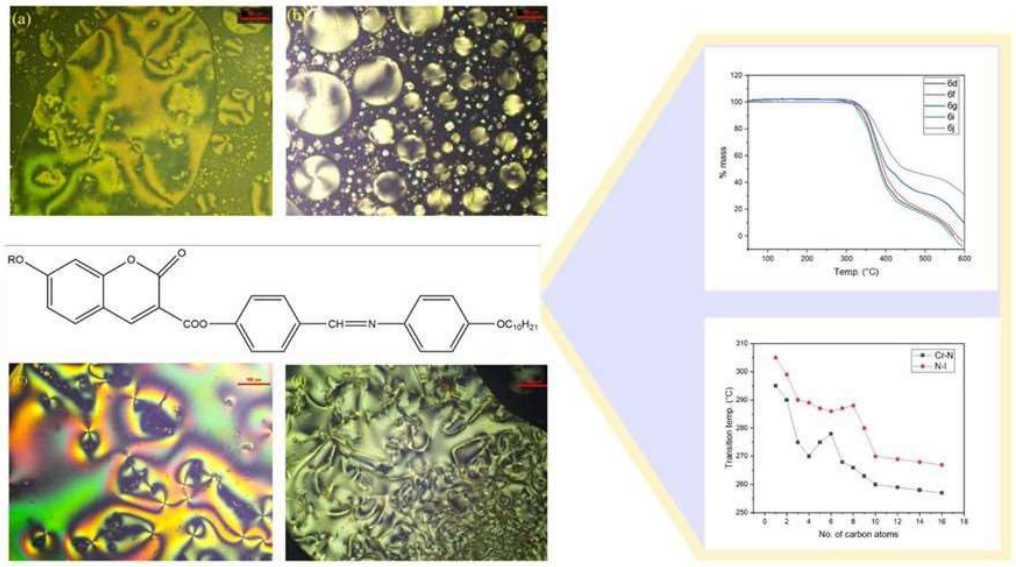

Synthesis, characterization, and study of nematogenic homologous series of coumarin derivatives containing azomethine-ester linkages

3.1. Introduction

A class of chemical molecules known as "coumarin derivatives" shares structural similarities with coumarin, a naturally occurring substance that is present in many different plants. By altering the coumarin structure, these derivatives are produced that have a variety of chemical and biological applications. The pharmacological effects of coumarin derivatives are well-known, and they have been thoroughly investigated for possible medical uses. Among other things, certain derivatives possess anticoagulant, anti-inflammatory, anticancer, antibacterial, and antioxidant activity. Coumarin derivatives are made up of α-pyrone ring and a benzene ring, but they can also have functional groups or other replacements attached to this basic structure and accordingly possess biological activities. To form novel coumarin derivatives with increased effectiveness and fewer adverse effects, a variety of synthetic techniques and modifications have been investigated. Due to their various biological functions and possible therapeutic uses, these derivatives are of great interest in medicinal chemistry.

Liquid crystalline coumarin derivatives have been found and developed as a result of continuing materials science and organic chemistry research. Researchers have been experimenting with changing coumarin structures to form substances with liquid crystal qualities. Researchers can modify the coumarin core's individual substituents or functional groups to change the molecule's physical characteristics, such as its ability to behave like a liquid crystal. Liquid crystalline coumarin derivatives are synthesized and studied using a combination of structural modifications, organic synthesis methods, and property evaluation. The goal of the research is to synthesize molecules with precise configurations that, in the presence of certain solvents or at particular temperatures and pressures, encourage the formation of liquid crystalline phases. To comprehend the liquid crystalline behavior, phase transitions, stability, and possible uses of these derivatives, a methodical procedure of designing, synthesizing, and characterizing compounds is used in their discovery and development. To modify the characteristics of these substances for specific uses in liquid crystal displays (LCDs), sensors, optical devices, or other technological breakthroughs, scientists research the links between molecular structure and property.

Tonka bean camphor, sometimes referred to as 1,2-benzopyrone, *2H*-1-benzopyran-2-one, phenylpropanoids, cis-o-coumarinic acid lactone, or coumarinic anhydride, is a member of a large class of chemicals that are widely distributed in bacteria, fungi, and plants [1, 2]. Tonka beans (family Fabaceae) are known by this colloquial name, which is derived from the French word "Coumarou" [3, 4]. The maximum concentration of coumarins can be found in the following plant parts: roots (Ferulago campestris), seeds (tonka beans, Calophylluminophyllum Linn), fruits (Bael fruit, Aegle marmeleos), and leaves (Murraya paniculata) [5-7].

Currently, one of the most significant fields of antibacterial research is the design of novel chemicals to deal with resistant bacteria, as the resistance of pathogenic bacteria to current antibiotics is rapidly becoming a major global concern. Moreover, the growing number of immunocompromised individuals is contributing to the rapid rise in the most serious and opportunistic fungal infections. As is well known, the primary obstacle to creating safe and effective antifungals is not only the biochemical similarity between human cells and fungi, which hinders their ability to exhibit selective activity but also the ease with which resistance can be developed [8]. Several novel 3-cinnamoyl-4-hydroxycoumarins were synthesized by Wan *et al*. [9] and their microbial activity was assessed using the disc diffusion and dilution techniques. Gram-negative bacteria showed resistance to the investigated drugs. The substances with halogen groups showed outstanding microbiological activity. For example, it was discovered that compounds with bromo and chloro-groups at the fourth position were the most effective against *B. subtilis.* It was found that compound (I), which has a chloro group at position four, is the most effective against *S. Aureus.*

However, 4-aryl-2,6-di(coumarin-3-yl)pyridine was synthesized by Patel *et al*. [10] and tested for antibacterial activity against *A. niger*. The gram-positive bacteria *B. subtilis* was moderately inhibited by the same chemicals. Furthermore, several novel 4-aryloxy methyl coumarins have been synthesized and published by Areti and Sandhu *et al*. [11, 12] who have also investigated the compounds antibacterial efficacy against five bacterial and five fungus species. Compounds (II) and (III) on the list have demonstrated exceptionally strong antibacterial activity against the strains that were tested.

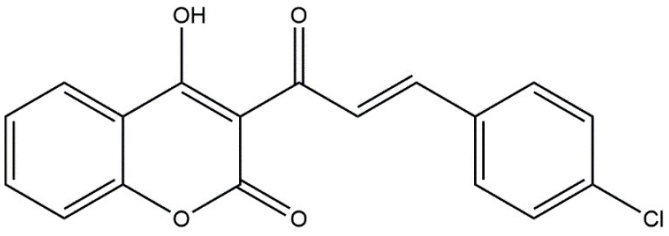

(I)

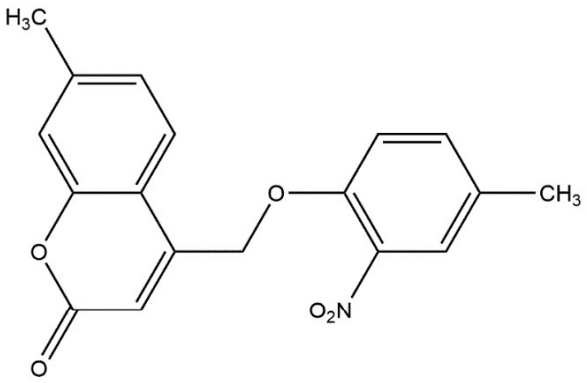

(II)

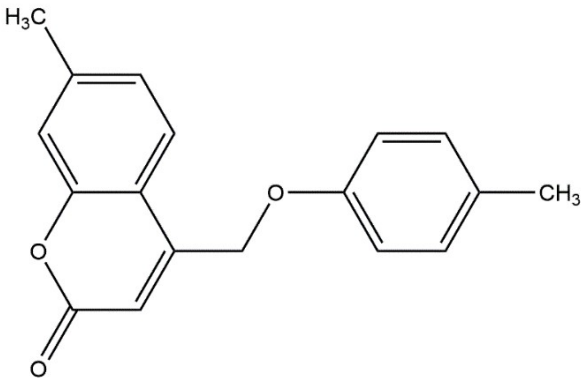

(III)

Figure 3.1: Coumarin derivatives possessing antimicrobial activity

The primary use of thermotropic rod-like liquid crystals (LCs) is being investigated for liquid crystal displays in a variety of electronic devices, including computer monitors, LCD televisions, digital calculators, digital clocks, digital cameras, mobile phones, and so on [13-16]. However, the combination of liquid crystalline and light-emitting features is necessary for the application of thermotropic rod-like LCs as optoelectronic devices [17-19]. Either simple or supramolecular emitting compounds can be designed, or emissive materials, such as

fluorescent dyes, can be used as a dopant with liquid crystalline solids [20, 21]. Enhancing optoelectronic characteristics by combining liquid crystalline and intrinsic emission properties in a single molecule is the key recent challenge in the thermotropic rod-like LCs sector. π-extended heterocycles, such as thiophene, coumarin, alkoxybenzene, benzooxazoles, benzothidiazoles, and so on, are essential in liquid crystals because they act as an anisometric core to produce mesomorphic properties and one-dimensional charge transfer to provide emissive properties [22–34]. However, aggregation-induced quenching (ACQ) during device construction resulted in very weak or nearly quenched emission properties of such compounds in the solid state.

It is simple to investigate the coumarin framework for the construction of various molecules that shed further light on the relationship between the liquid crystalline features of coumarins and their core [35-38]. Coumarin derivatives show very good fluorescence properties with large Stokes shift and narrow emission range. The type and position of the functional group have a significant impact on the emission properties of coumarin derivatives. Derivatives of coumarin have been employed as dopants in the production of liquid crystal materials based on fluorescent polymers. Small compounds based on coumarins have recently been investigated as a potential source of emissive liquid crystal materials. Photoemissive coumarin derivative (IV) with stable nematic and SmA mesophases has been described by Merlo *et al*. [39]. Two series of derivatives (V) with photoluminescence capabilities have been described by Mustafa and Mohammed [40] as liquid crystalline unsymmetrical dimeric compounds comprising coumarin heterocyclic rings connected to chalcone alkyl substitution via ether group. Due to the general change in polarity and orientation of dipole moments, it was discovered that changes in connecting groups and length terminal alkoxy chain had a significant impact on the mesomorphic properties of 7-alkoxy 3-amino coumarin. Our group studies the substantial effects of the terminal polar group on the mesomorphic properties of the coumarin Schiff-base.

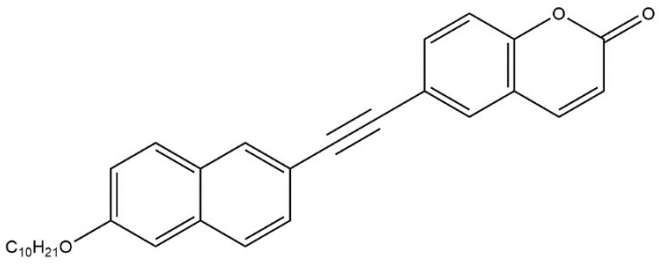

(IV)

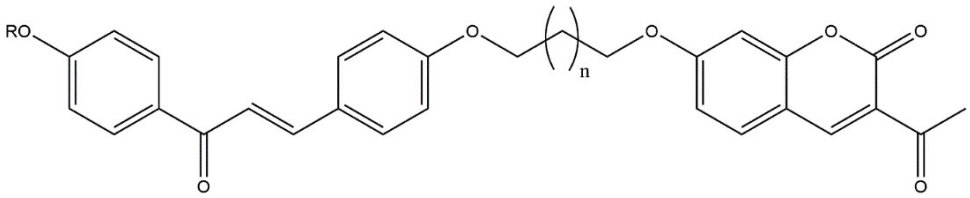

n = 2, 4
R = C_6H_{13} to $C_{14}H_{29}$

(V)

Figure 3.2: Thermotropic liquid crystals with photoluminescence properties

The characteristics of both liquid and crystal are present in liquid crystalline material. These materials were first used in liquid crystal displays because of their dual characteristics. Liquid crystalline material has recently found use in optical storage, chemical and biological sensors, and liquid crystal thermometers. The demand to develop new liquid crystalline materials, particularly those of the thermotropic class, has increased due to the vast range of uses of these materials. Six alkyl chains are found in a flexible terminal core of a rod-like thermotropic liquid crystal material, while phenyl rings are found in a rigid core [41-46]. Coumarin ester derivatives have been reported as liquid crystalline substances by Trivedi *et al*. and Dave *et al*. With ester linkage, Srinivasa *et al*. synthesized ethyl 7-hydroxycoumarin-3-carboxylate derivatives (VIII) and (IX), which demonstrated good liquid crystalline behavior possessing smectic and nematic phases. Hagar *et al*. have reported 7-hydroxy-4-methyl-coumarin derivatives (VI) and (VII) with ester and azo-ester.

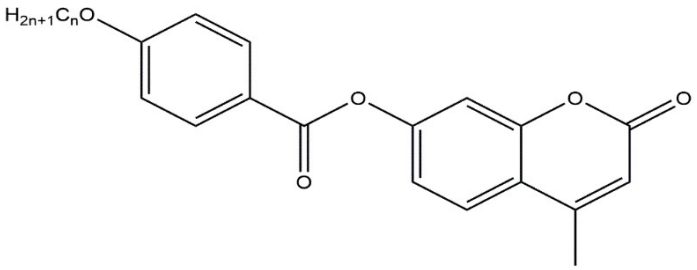

n = 6, 8, 10, 12, and 16

(VI)

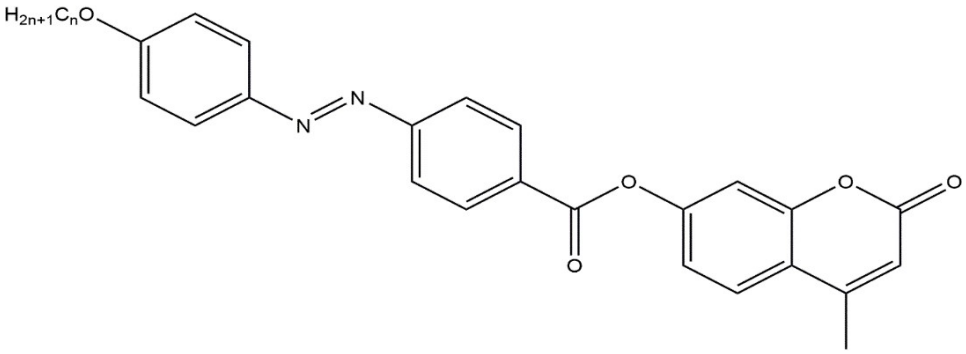

n = 6, 8, 10, 12, and 16

(VII)

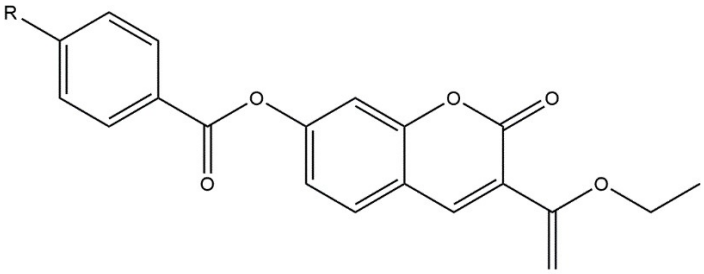

R = $-OC_9H_{19}$, $-OC_{18}H_{37}$

(VIII)

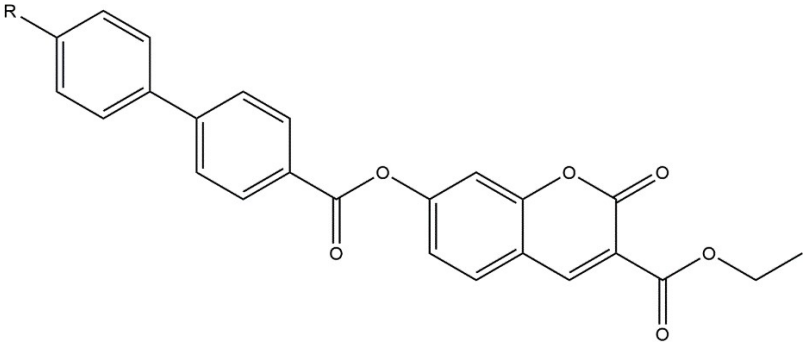

R = $-C_6H_{13}$, $-C_8H_{17}$, $-C_{12}H_{25}$

(IX)

Figure 3.3: Coumarin liquid crystalline derivatives

Inducing unique features in Schiff bases, azomethanes, heterocyclic compounds, coumarin skeletons, and related molecular structures is a difficult undertaking [47-51]. The aforementioned molecules have been the subject of a great deal of research, and valuable information about liquid crystal mesomorphism has been noted [52-55]. Various studies have been conducted on the compounds, and important insights into liquid crystal mesomorphism have been observed. In monomeric coumarin derivatives, the kind of mesophase is determined by the molecular structures and the kinds of groups that are replaced at various points. Many research groups are working on the synthesis and studies of monomers and dimers derived from various heterocyclic compounds with azo/imine/Schiff base linkages for the interesting liquid crystal behavior with a variety of mesophases to continue the evaluation of heterocyclic cores for LC properties [56-60].

In recent years, enhancements in the research of coumarin derivatives have been found due to its wide range of applications in the field of organic light-emitting diodes (OLEDs), light harvesting materials, chemosensors, photorefractive materials, non-linear optical materials and photo alignment of mesomorphic material possessing photochemical and photophysical properties. Coumarin moiety is considered a very essential component due to its polarity and a significant dipole moment (5.48 D) and is hence responsible for mesomorphic as well as electronic properties [61]. Coumarin derivatives have a very wide range of applications in biological and display systems [62]. Different linking groups such as ester, imine, etc. at the core position of the moiety enhance the mesomorphism. Yan Li, *et al* have developed novel heterocyclic mesomorphic compounds comprising smectic and nematic phases [63]. Coumarins are considered as a very essential component and are used in the synthesis of drugs due to their various characteristics including high solubility and low molecular weight [64-66]. Numerous significant photophysical characteristics of coumarin-containing compounds make them useful molecules for fluorescent sensors, optical devices, fluorescence dyes, laser dyes, organic light-emitting diodes (LED), and chemosensors. It is commonly recognized that the molecular architectures of rod-shaped liquid crystal materials (LCs) determine their physico-chemical properties. With the interest in these structures increasing steadily, numerous liquid crystal compounds based on coumarin derivatives have recently been reported. There has been a lot of recent reporting of liquid crystal compounds based on coumarin derivatives, and interest in these structures is gradually increasing. The synthesis and investigation of thermotropic liquid crystals based on heterocyclic scaffolds continue to be a noteworthy and stimulating aspect of the expanding body of research in this area. Although a lot of research has been done

in the liquid crystal field, the application of naturally occurring compounds based on coumarins that contain Schiff base/ester linking units has been studied. Adding molecules based on coumarins to the mesogen spectrum is essential for several physical attributes. Heterocyclic coumarin-based compounds are highly sought after due to their prospective applications as opto- and electro-active materials.

In this chapter, we report the synthesis of compounds containing Schiff's Base and coumarin moiety incorporated in a molecule with an alkoxy group (n = 1-10, 12, 14, 16) attached at one of the terminal ends and n-decyloxy at another terminal end of the molecule. The optical textures and the phase temperatures were confirmed by using POM and DSC. The thermal behavior was assessed by thermogravimetric analysis. The structure-mesomorphic relationship was carefully studied. The photophysical properties have been carefully studied. All the synthesized compounds were screened for their in-vitro antibacterial activity against *Escherichia Coli* and *Staphylococcus aureus* showing good to moderate activity compared to the used standard.

3.2. Experimental Section

3.2.1 Materials and Measurements

The synthetic strategy for all the synthesized coumarin derivatives was elucidated in Scheme 3.1. The proposed structures of all the newly prepared compounds were confirmed by FT-IR, ^{1}H-NMR, ^{13}C-NMR, and elemental analysis.

All the chemicals and solvents were purchased from Sigma Aldrich and used in a reaction without further purification. 2,4-dihydroxybenzaldehyde, p-hydroxybenzaldehyde from Sigma Aldrich, pyridine, potassium carbonate, potassium hydroxide, thionyl chloride, NaOH, absolute alcohol, and glacial acetic acid from Lobachemie Pvt. Ltd., Diethyl malonate, piperidine, n-alkyl bromide, 4-n-hydroxyacetanilide from Spectrochem Pvt. Ltd., acetone and dimethyl formamide from SD Fine Chem. Limited. Thin Layer Chromatography (TLC) was performed on aluminum silica gel plates (Merck 60 F245) with examination under UV light. FT-IR spectra were determined for KBr pellets using a Perkin Elmer Spectrum Two. Using ^{1}H NMR and ^{13}C NMR spectrum data were recorded in an Avance Bruker 400 spectrophotometer (400 MHz & 150 MHz, respectively) with TMS as an internal standard and deuterated chloroform ($CDCl_3$) as the solvent. Nikon Eclipse C*i*-Pol microscope (Japan) equipped with a Linkam heating stage (to determine the transition temperatures of prepared compounds),

differential scanning calorimetry (DSC-822, Mettler Toledo having Stare software) with platinum pans, 4-5 mg sample amount with 30–40 mL min^{-1} nitrogen gas inert atmosphere and 10 °C min^{-1} heating rate were used to study the thermal behavior of prepared compounds. About 2-3 mg of the sample was taken in a thermogravimetric analyzer (TGA-50, Shimadzu Japan), to measure the thermal stability of the compounds. Thermo Finnigan (Flash 1112 series EA) CHN analyzer was used to carry out an elemental analysis. A photoluminescence study was carried out using a Shimadzu RF-6000 spectrofluorometer (Japan). Using the DFT/B3LYP approach, Orca 5.0 [Functional - B3LYP, Basis set - def-TZVP, RIJCOSX] software performed all of the theoretical computations for the synthesized compounds.

3.2.2 Synthesis and Characterization

3.2.2.1 Synthesis of Ethyl 7-hydroxycoumarin-3-carboxylates (1)

2,4-dihydroxybenzaldehyde (0.1 mol), diethyl malonate (0.1 mol), 5 mL of dry pyridine, and a few drops of piperidine were mixed and left overnight. The reaction mixture was treated with dilute HCl. The product obtained was cleaned and purified using appropriate solvent [67]. Melting Point: 170 °C.

3.2.2.2 Synthesis of Ethyl 7-n-alkoxycoumarin-3-carboxylates (2a-2m)

Ethyl 7-n-hydroxycoumarin-3-carboxylate (0.01 mol), n- alkyl bromide (0.012 mol), potassium carbonate (0.07 mol), and 15 mL of dimethyl formamide were mixed and heated on steam bath for 20 h. The reacted mixture was poured into crushed ice. The product obtained was cleaned and purified using appropriate solvent [68].

3.2.2.3 Synthesis of 7-n-alkoxycoumarin-3-carboxylic acids (3a-3m)

Ethyl 7-n-alkoxycoumarin-3-carboxylates (0.01 mol) were dissolved in 40 mL 10% of alcoholic potassium hydroxide and left overnight. The reaction mixture was poured into ice-cold dilute hydrochloric acid. The product obtained was cleaned and purified using appropriate solvent [69].

3.2.2.4 Synthesis of 4'-formylphenyl-7-n-alkoxycoumarin-3-carboxylates (4a-4m)

The corresponding 7-n-alkoxycoumarin-3-carboxylic acids were treated with excess thionyl chloride and 7-n-alkoxycoumarin-3-carboxylic acid chlorides which was further treated with equimolar quantities of p-hydroxybenzaldehyde (0.005 mol) in 5-7 mL of dry pyridine and heated on a water bath for an hour and left overnight. The reaction mixture was then added to ice-cold dilute hydrochloric acid. The product was washed with dilute NaOH and water. The product was recrystallized from a mixture of ethanol containing a few drops of benzene [70].

3.2.2.5 Synthesis of 4-n-decyloxyaniline (5)

4-n-hydroxy acetanilide (0.1 mol), anhydrous potassium carbonate (0.1 mol), and dry acetone (60 mL) were heated at 70-80 °C and to the warm solution, the appropriate alkyl halide was added dropwise for 1 h. The mixture was refluxed with continuous stirring at 70-80 °C for 8-10 h. The reaction mixture was diluted with cold water. The product obtained was filtered, washed with water, and directly used for hydrolysis under appropriate conditions [71]. Yield obtained: 80-85%. Melting Point: 65.2 °C.

3.2.2.6 Synthesis of 4'-(4''-n-decyloxyphenyl iminomethyl)phenyl, 7-n-alkoxy-2-oxo-4[*H*]-chromene-3-carboxylate(6a-6m) [Series-I]

4'-formylphenyl-7-n-alkoxycoumarin-3-carboxylates (0.1 mol) were treated with 4-n-decyloxyaniline (0.1 mol) using absolute alcohol (10-12 mL) and glacial acetic acid as a catalyst. Refulx was carried out for 3 h. The product obtained was recrystallized from ethanol. Yield obtained was around 72-79%.

4'-(4''-n-decyloxyphenyl iminomethyl)phenyl, 7-n-methoxy-2-oxo-4[*H*]-chromene-3-carboxylate (6a)

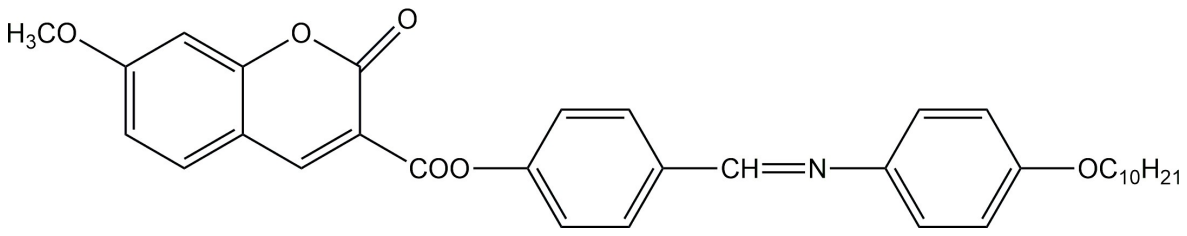

Yellow crystal, yield 73.2%. **FT-IR** (cm^{-1}): 2922, 2853 (C-H, aliphatic), 1768 (C=O in ester), 1715 (O-C=O, cyclic ester), 1600 (-C=N), 1506 (C = C, aromatic), 1292, 1251 (R-O-Ar, ether), 1018, 835, (C-H, aromatic). **^{1}H NMR** (400 MHz, $CDCl_3$) δ (ppm): 8.74 (s, 1H, Ar-H), 8.52 (s,

1H, -CH=N-), 7.96-7.58 (d, 3H, J = 8.4 Hz, Ar-H), 7.58-7.36 (d, 2H, J = 8.8 Hz, Ar-H), 6.97 (s, 1H, Ar-H), 6.94 (d, 1H, J = 2.4 Hz, Ar-H), 6.93-6.86 (d, 4H, J = 2.2 Hz, Ar-H), 4.10-4.02 (t, 2H,-O-CH_2-), 1.85-1.07 (m, 16H, -CH_2-CH_2-), 0.91-0.87 (t, 6H, -CH_2-CH_3). **^{13}C NMR** (150 MHz, $CDCl_3$) δ (ppm): 165.5 (- C=O), 161.4 (-CH=N-), 144.5 (-C-N), 158.1, 158.0, 156.8, 152.7, 150.4, 134.3, 131.1, 129.8, 122.1, 122.0, 115.2, 114.9, 112.5, 100.9, 100.8 (Ar-C), 69.3, 69.1 (Ar-O-CH_2-), 31.8, 31.3, 29.6, 29.4, 29.5, 29.2, 28.7, 26.6, 25.4 (-CH_2-CH_2-), 22.7, 22.6 (-CH_2-CH_3), 14.6, 14.5 (-CH_2-CH_3).

4'-(4''-n-decyloxyphenyl iminomethyl)phenyl, 7-n-ethoxy-2-oxo-4[*H*]-chromene-3-carboxylate (6b)

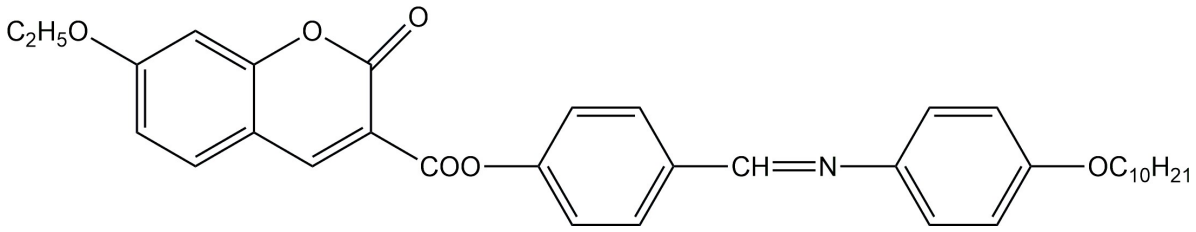

Light brown crystal, yield 75.11%. **FT-IR** (cm^{-1}): 2920, 2852 (C-H, aliphatic), 1759 (C=O in ester), 1714 (O-C=O, cyclic ester), 1616 (C=N), 1556, 1508 (C = C, aromatic), 1256, 1215, 1203 (R-O-Ar, ether), 1003, 990, 860, 788 (C-H, aromatic). **^{1}H NMR** (400 MHz, $CDCl_3$) δ (ppm): 8.75 (s, 1H, Ar-H), 8.51 (s, 1H, -CH=N-), 7.95-7.57 (d, 3H, J = 8.8 Hz, Ar-H), 7.56-7.35 (d, 2H, J = 8.4 Hz, Ar-H), 6.96 (s, 1H, Ar-H), 6.95 (d, 1H, J = 2.4 Hz, Ar-H), 6.92-6.85 (d, 4H, J = 2.4 Hz, Ar-H), 4.09-4.04 (t, 4H,-O-CH_2-), 1.86-1.08 (m, 16H, -CH_2-CH_2-), 0.92-0.86 (t, 6H, -CH_2-CH_3). **^{13}C NMR** (150 MHz, $CDCl_3$) δ (ppm): 165.4 (-C=O), 161.4 (-CH=N-), 144.1 (-C-N), 158.2, 158.0, 156.9, 152.6, 150.5, 134.2, 131.2, 129.7, 122.2, 122.0, 115.1, 114.7, 114.2, 111.5, 100.9, 100.8 (Ar-C), 69.2, 69.0 (Ar-O-CH_2-), 31.8, 31.3, 29.6, 29.4, 29.5, 29.2, 28.7, 26.6, 25.4 (-CH_2-CH_2-), 22.7, 22.6 (-CH_2-CH_3), 14.6, 14.5 (-CH_2-CH_3).

4'-(4''-n-decyloxyphenyl iminomethyl)phenyl, 7-n-propoxy-2-oxo-4[*H*]-chromene-3-carboxylate (6c)

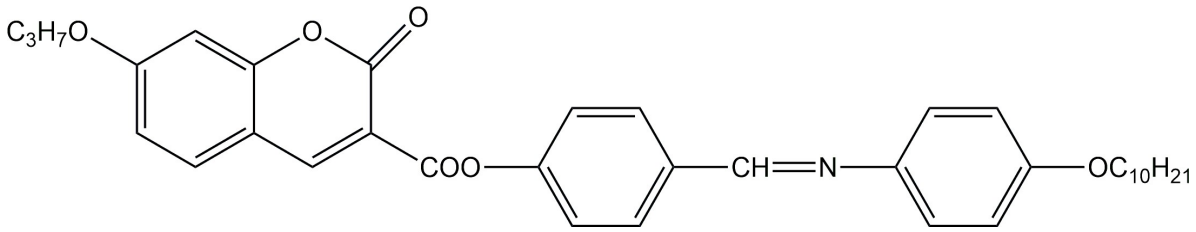

Light yellow crystal, yield 76.58%. **FT-IR** (cm^{-1}): 2964, 2955, 2920, 2872, 2852 (C-H, aliphatic), 1768 (C=O in ester), 1716 (O-C=O, cyclic ester), 1620 (C=N), 1560, 1506 (C = C, aromatic), 1298, 1276, 1246, 1222 (R-O-Ar, ether), 1014, 962, 831, 790 (C-H, aromatic). **^{1}H NMR** (400 MH_Z, $CDCl_3$) δ (ppm): 8.76 (s, 1H, Ar-H), 8.52 (s, 1H, -CH=N-), 7.94-7.56 (d, 3H, J = 8.4 Hz, Ar-H), 7.57-7.34 (d, 2H, J = 8.8 Hz, Ar-H), 6.96 (s, 1H, Ar-H), 6.94 (d, 1H, J = 2 Hz, Ar-H), 6.93-6.85 (d, 4H, J = 2 Hz, Ar-H), 4.10-4.06 (t, 4H,-O-CH_2-), 1.86-1.08 (m, 18H, -CH_2-CH_2-), 0.92-0.86 (t, 6H, -CH_2-CH_3). **^{13}C NMR** (150 MHz, $CDCl_3$) δ (ppm): 165.4 (-C=O), 161.4 (-CH=N-), 144.1 (-C-N), 158.2, 158.0, 156.9, 152.6, 150.5, 134.2, 131.2, 129.7, 122.2, 122.0, 115.1, 114.7, 114.2, 111.5, 100.9, 100.8 (Ar-C), 69.2, 69.0 (Ar-O-CH_2-), 31.8, 31.3, 29.6, 29.4, 29.5, 29.2, 28.7, 26.6, 25.4 (-CH_2-CH_2-), 22.7, 22.6 (-CH_2-CH_3), 14.6, 14.5 (-CH_2-CH_3).

4'-(4''-n-decyloxyphenyl iminomethyl)phenyl, 7-n-butoxy-2-oxo-4[*H*]-chromene-3-carboxylate (6d)

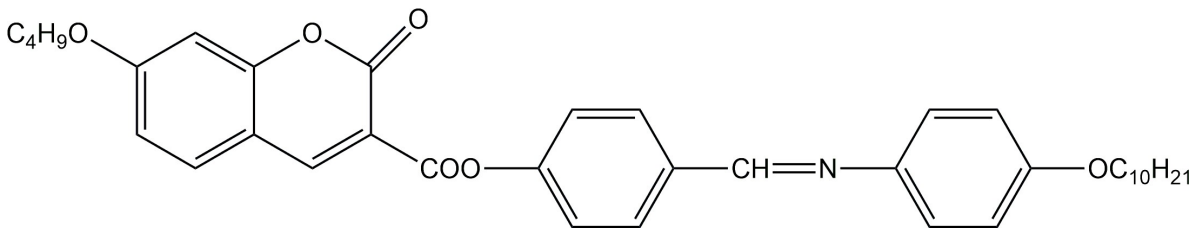

Light yellow crystal, yield 76.15%. **FT-IR** (cm^{-1}): 2951, 2924, 2920, 2888, 2850 (C-H, aliphatic), 1766 (C=O in ester), 1714 (O-C=O, cyclic ester), 1606 (C=N), 1554, 1504 (C = C, aromatic), 1276, 1246, 1219 (R-O-Ar, ether), 1031, 1012, 995, 889, 833, 788 (C-H, aromatic). **^{1}H NMR** (400 MH_Z, $CDCl_3$) δ (ppm): 8.75 (s, 1H, Ar-H), 8.51 (s, 1H, -CH=N-), 7.99-7.59 (d, 3H, J = 8.8 Hz, Ar-H), 7.57-7.37 (d, 2H, J = 8.8 Hz, Ar-H), 6.96 (s, 1H, Ar-H), 6.95 (d, 1H, J = 2 Hz, Ar-H), 6.94-6.85 (d, 4H, J = 2 Hz, Ar-H), 4.11-4.01 (t, 4H,-O-CH_2-), 1.87-1.09 (m, 20H, -CH_2-CH_2-), 0.92-0.88 (t, 6H, -CH_2-CH_3). **^{13}C NMR** (150 MHz, $CDCl_3$) δ (ppm): 165.4 (-C=O), 161.1 (-CH=N-), 144.4 (-C-N), 158.1, 156.9, 156.8, 152.6, 150.5, 134.4, 131.2, 131.0, 129.7, 122.5, 122.1, 115.0, 114.8, 114.6, 114.3, 112.5, 111.4, 100.8, 100.7 (Ar-C), 68.8, 68.7 (Ar-O-CH_2-), 31.9 30.8, 29.6, 29.5, 29.4, 29.3, 28.0, 27.6, 26.0 (-CH_2-CH_2-), 22.6, 19.1 (-CH_2-CH_3), 14.1, 13.7 (-CH_2-CH_3).

4'-(4''-n-decyloxyphenyl iminomethyl)phenyl, 7-n-pentoxy-2-oxo-4[*H*]-chromene-3-carboxylate (6e)

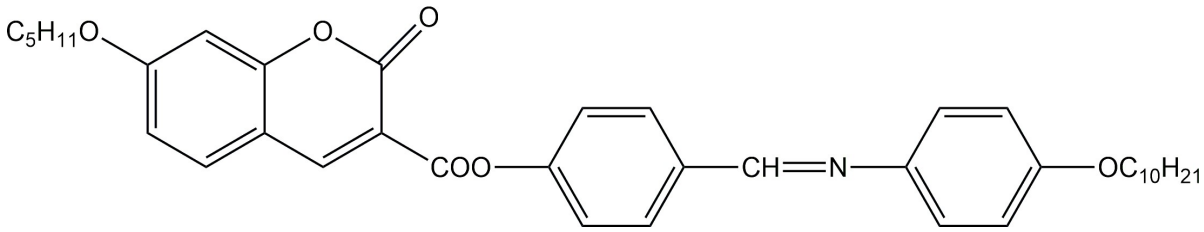

Yellow crystal, yield 75.10%. **FT-IR** (cm^{-1}): 2952, 2920, 2915, 2885, 2855 (C-H, aliphatic), 1760 (C=O in ester), 1715 (O-C=O, cyclic ester), 1610 (C=N), 1550, 1510 (C = C, aromatic), 1250, 1220 (R-O-Ar, ether), 1021, 1014, 990, 885, 830, 785 (C-H, aromatic). **^{1}H NMR** (400 MH_Z, $CDCl_3$) δ (ppm): 8.74 (s, 1H, Ar-H), 8.52 (s, 1H, -CH=N-), 7.98-7.60 (d, 3H, J = 8.4 Hz, Ar-H), 7.59-7.36 (d, 2H, J = 8.4 Hz, Ar-H), 6.94 (s, 1H, Ar-H), 6.96 (d, 1H, J = 2 Hz, Ar-H), 6.94-6.86 (d, 4H, J = 2.4 Hz, Ar-H), 4.10-4.02 (t, 4H,-O-CH_2-), 1.88-1.09 (m, 22H, -CH_2-CH_2-), 0.92-0.88 (t, 6H, -CH_2-$C\underline{H}_3$). **^{13}C NMR** (150 MHz, $CDCl_3$) δ (ppm): 165.5 (-C=O), 161.1 (-CH=N-), 144.2 (-C-N), 158.2, 156.8, 156.7, 152.5, 150.4, 134.5, 131.2, 131.0, 129.6, 122.6, 122.2, 115.0, 114.8, 114.6, 114.3, 112.5, 111.4, 100.8, 100.7 (Ar-C), 68.8, 68.7 (Ar-O-CH_2-), 31.9, 30.8, 29.6, 29.5, 29.4, 29.3, 28.0, 27.6, 26.0 (-CH_2-CH_2-), 22.6, 19.1 (-$\underline{C}H_2$-CH_3), 14.1, 13.7 (-CH_2-$\underline{C}H_3$).

4'-(4''-n-decyloxyphenyl iminomethyl)phenyl, 7-n-hexyloxy-2-oxo-4[*H*]-chromene-3-carboxylate (6f)

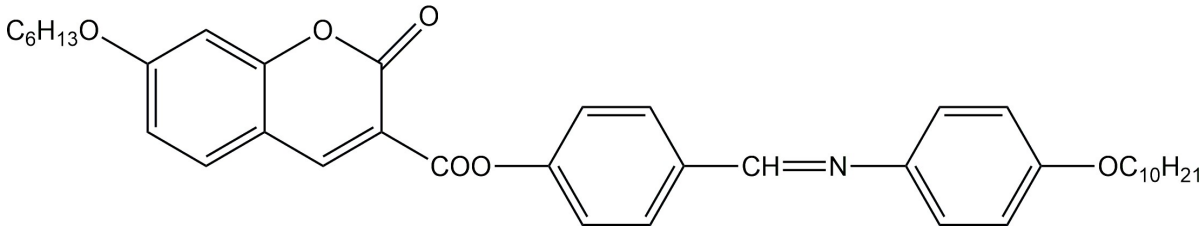

Light Brown crystal, yield 73.48%. **FT-IR** (cm^{-1}): 2951, 2922, 2866, 2850 (C-H, aliphatic), 1739 (C=O in ester), 1714 (O-C=O, cyclic ester), 1606 (C=N), 1556, 1504 (C = C, aromatic), 1261, 1249, 1219 (R-O-Ar, ether), 1016, 891, 827, 788 (C-H, aromatic). **^{1}H NMR** (400 MH_Z, $CDCl_3$) δ (ppm): 8.75 (s, 1H, Ar-H), 8.50 (s, 1H, -CH=N-), 7.98-7.58 (d, 3H, J = 8.8 Hz, Ar-H), 7.56-7.34 (d, 2H, J = 8.8 Hz, Ar-H), 6.96 (s, 1H, Ar-H), 6.95 (d, 1H, J = 2.4 Hz, Ar-H), 6.94-6.85 (d, 4H, J = 2 Hz, Ar-H), 4.09-4.01 (t, 4H,-O-CH_2-), 1.89-1.29 (m, 24H, -CH_2-CH_2-), 0.95-0.88 (t, 6H, -CH_2-$C\underline{H}_3$). **^{13}C NMR** (150 MHz, $CDCl_3$) δ (ppm): 165.4 (-C=O), 161.6 (-

CH=N-), 144.4 (-C-N), 158.0, 158.1, 156.9, 152.6, 150.5, 134.4, 131.0, 129.7, 122.2, 122.0, 115.0, 114.8, 114.6, 114.3, 112.4, 111.4, 100.8, 100.7 (Ar-C), 69.1, 69.0 (Ar-O-CH_2-), 31.9, 31.4, 29.5, 29.5, 29.4, 29.3, 28.8, 26.0, 25.5 (-CH_2-CH_2-), 22.6, 22.5 (-$\underline{C}H_2$-CH_3), 14.1, 14.0 (-CH_2-$\underline{C}H_3$).

4'-(4''-n-decyloxyphenyl iminomethyl)phenyl, 7-n-heptyloxy-2-oxo-4[*H*]-chromene-3-carboxylate (6g)

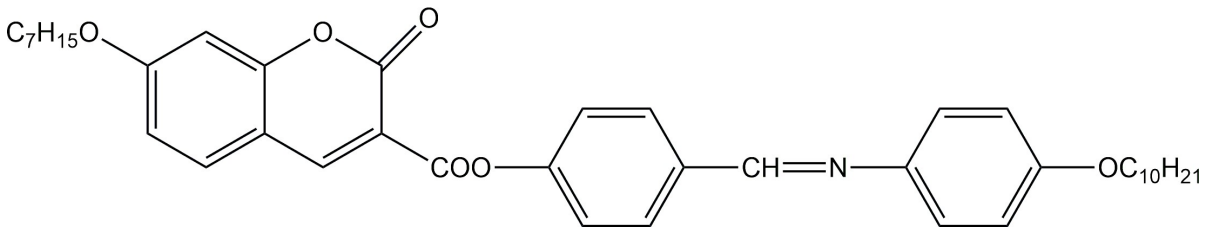

Colourless needle-like crystal, yield 78.50%. **FT-IR** (cm^{-1}): 2953, 2922, 2868, 2852 (C-H, aliphatic), 1741 (C=O in ester), 1714 (O-C=O, cyclic ester), 1606 (C=N), 1506 (C = C, aromatic), 1246, 1215 (R-O-Ar, ether), 1014, 960, 829, 790 (C-H, aromatic). **^{1}H NMR** (400 MH_Z, $CDCl_3$) δ (ppm): 8.75 (s, 1H, Ar-H), 8.51 (s, 1H, -CH=N-), 7.98-7.58 (d, 3H, J = 8.8 Hz, Ar-H), 7.56-7.37 (d, 2H, J = 8.4 Hz, Ar-H), 6.96 (s, 1H, Ar-H), 6.95 (d, 1H, J = 2.4 Hz, Ar-H), 6.94-6.85 (d, 4H, J = 2 Hz, Ar-H), 4.10-4.01 (t, 4H,-O-CH_2-), 1.89-1.29 (m, 26H, -CH_2-CH_2-), 0.94-0.88 (t, 6H, -CH_2-$\underline{C}H_3$). **^{13}C NMR** (150 MHz, $CDCl_3$) δ (ppm): 165.3 (-C=O), 161.7 (-CH=N-), 144.4 (-C-N), 158.0, 158.0, 156.9, 150.5, 134.4, 131.2, 131.0, 129.7, 122.5, 122.2, 122.1, 115.0, 114.3, 112.5, 111.4, 100.8 (Ar-C), 69.1, 68.3 (Ar-O-CH_2-), 31.9, 31.7, 29.5, 29.4, 29.3 , 28.9, 28.8, 26.0, 25.8 (-CH_2-CH_2-), 22.6, 22.5 (-$\underline{C}H_2$-CH_3), 14.0 (-CH_2-$\underline{C}H_3$).

4'-(4''-n-decyloxyphenyl iminomethyl)phenyl, 7-n-octyloxy-2-oxo-4[*H*]-chromene-3-carboxylate (6h)

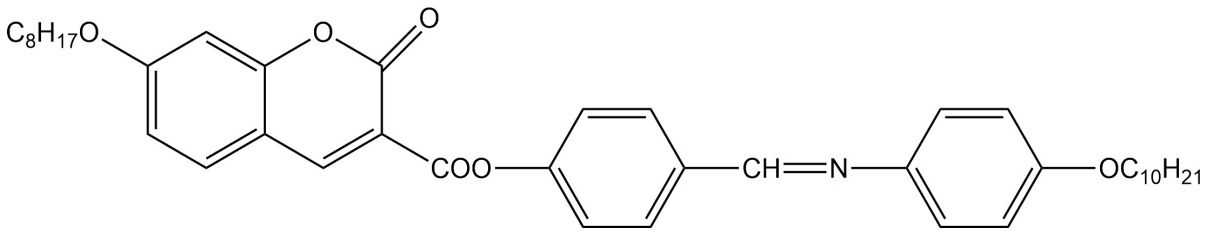

Yellow crystal, yield 78.06%. **FT-IR** (cm^{-1}): 2922, 2866, 2862 (C-H, aliphatic), 1764 (C=O in ester), 1716 (O-C=O, cyclic ester), 1604 (C=N), 1506 (C = C, aromatic), 1246, 1217 (R-O-Ar, ether), 1012, 950, 829, 790 (C-H, aromatic). **^{1}H NMR** (400 MH_Z, $CDCl_3$) δ (ppm): 8.76 (s, 1H,

Ar-H), 8.52 (s, 1H, -CH=N-), 7.99-7.59 (d, 3H, J = 8.4 Hz, Ar-H), 7.57-7.36 (d, 2H, J = 8.8 Hz, Ar-H), 6.97 (s, 1H, Ar-H), 6.96 (d, 1H, J = 2.4 Hz, Ar-H), 6.94-6.86 (d, 4H, J = 2.4 Hz, Ar-H), 4.09-4.05 (t, 4H,-O-CH_2-), 1.87-1.30 (m, 28H, -CH_2-CH_2-), 0.94-0.88 (t, 6H, -CH_2-CH_3). **^{13}C NMR** (150 MHz, $CDCl_3$) δ (ppm): 165.2 (-C=O), 161.8 (-CH=N-), 144.2 (-C-N), 158.7, 158.6, 156.8, 150.4, 134.2, 131.1, 131.0, 129.7, 129.6, 129.5, 122.6, 122.5, 122.3, 122.2, 122.1, 115.0, 114.3, 112.5, 111.4, 100.8 (Ar-C), 69.1, 68.3 (Ar-O-CH_2-), 31.9, 31.7, 31.6, 29.5, 29.4 , 29.3, 28.9, 28.8, 26.0, 25.8 (-CH_2-CH_2-), 22.6, 22.5 (-CH_2-CH_3), 14.0 (-CH_2-CH_3).

4’-(4’’-n-decyloxyphenyliminomethyl)phenyl,7-n-nonyloxy-2-oxo-4[*H*]-chromene-3-carboxylate (6i)

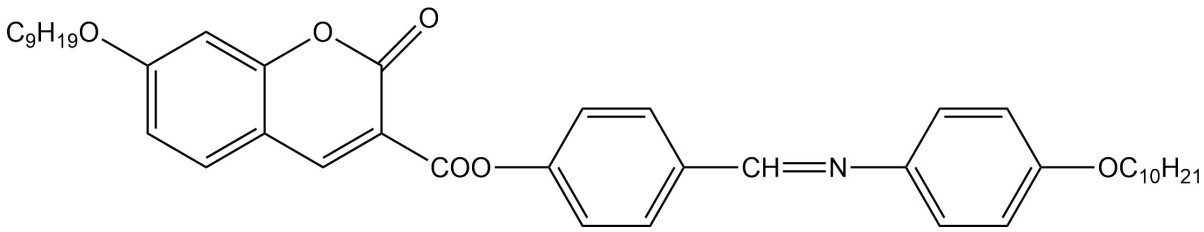

Light yellow crystal, yield 79.51%. **FT-IR** (cm^{-1}): 2922, 2852 (C-H, aliphatic), 1764 (C=O in ester), 1716 (O-C=O, cyclic ester), 1620 (C=N), 1560, 1506 (C = C, aromatic), 1246, 1217 (R-O-Ar), 1012, 958, 862, 827, 792 (C-H, aromatic). **^{1}H NMR** (400 MHz, $CDCl_3$) δ (ppm): 8.75 (s, 1H, Ar-H), 8.51 (s, 1H, -CH=N-), 7.98-7.59 (d, 3H, J = 8.4 Hz, Ar-H), 7.56-7.35 (d, 2H, J = 8.4 Hz, Ar-H), 6.96 (s, 1H, Ar-H), 6.95 (d, 1H, J = 2.4 Hz, Ar-H), 6.94-6.86 (d, 4H, J = 2.4 Hz, Ar-H), 4.10-4.01 (t, 4H,-O-CH_2-), 1.89-1.29 (m, 30H, -CH_2-CH_2-), 0.92-0.88 (t, 6H, -CH_2-CH_3). **^{13}C NMR** (150 MHz, $CDCl_3$) δ (ppm): 165.5 (-C=O), 161.8 (-CH=N-), 144.5 (-C-N), 158.1, 158.0, 156.9, 150.5, 131.0, 129.7, 122.2, 122.1, 115.0, 114.8, 114.4, 100.8 (Ar-C), 69.1, 68.3 (Ar-O-CH_2-), 31.9, 31.8, 29.5, 29.4, 29.3, 29.2, 28.8, 26.0, 25.9 (-CH_2-CH_2-), 22.6 (-CH_2-CH_3), 14.1 (-CH_2-CH_3).

4’-(4’’-n-decyloxyphenyl iminomethyl)phenyl, 7-n-decyloxy-2-oxo-4[*H*]-chromene-3-carboxylate (6j)

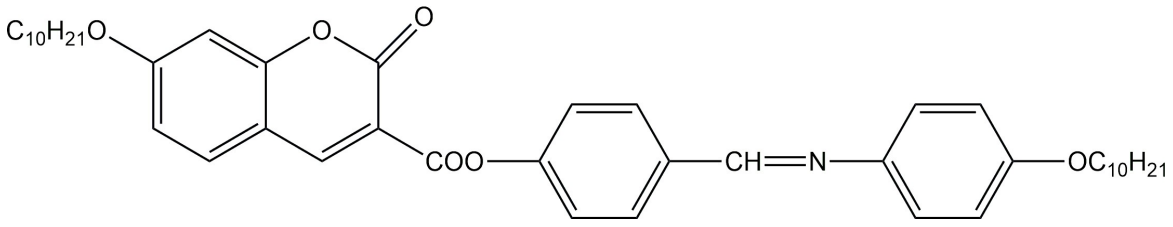

Off-white crystal, yield 72.73%. **FT-IR** (cm^{-1}): 2955, 2922, 2850 (C-H, aliphatic), 1763 (C=O in ester), 1716 (O-C=O, cyclic ester), 1618 (C=N), 1555, 1506 (C = C, aromatic), 1246, 1217 (R-O-Ar, ether), 1010, 959, 829, 790 (C-H, aromatic). **^{1}H NMR** (400 MH_Z, $CDCl_3$) δ (ppm): 8.75 (s, 1H, Ar-H), 8.51 (s, 1H, -CH=N-), 7.98-7.58 (d, 3H, J = 8.8 Hz, Ar-H), 7.56-7.35 (d, 2H, J = 8.8 Hz, Ar-H), 6.96 (s, 1H, Ar-H), 6.95 (d, 1H, J = 2.4 Hz, Ar-H), 6.94-6.85 (d, 4H, J = 2 Hz, Ar-H), 4.10-4.01 (t, 4H,-O-CH_2-), 1.89-1.29 (m, 32H, -CH_2-CH_2-), 0.92-0.88 (t, 6H, -CH_2-CH_3). **^{13}C NMR** (150 MHz, $CDCl_3$) δ (ppm): 165.3 (-C=O), 161.9 (-CH=N-), 144.2 (-C-N), 158.3, 158.3, 156.8, 150.4, 131.3, 129.8, 122.4, 122.5, 115.1, 115.0, 114.8, 114.4, 100.8 (Ar-C), 69.1, 68.3 (Ar-O-CH_2-), 31.9, 31.8, 31.8, 30.9, 30.7, 30.5, 29.5, 29.4, 29.3, 29.2, 29.1, 28.8, 28.7, 26.0, 25.9, 25.8 (-CH_2-CH_2-), 22.6 (-CH_2-CH_3), 14.1 (-CH_2-CH_3).

4'-(4''-n-decyloxyphenyl iminomethyl)phenyl, 7-n-dodecyloxy-2-oxo-4[*H*]-chromene-3-carboxylate (6k)

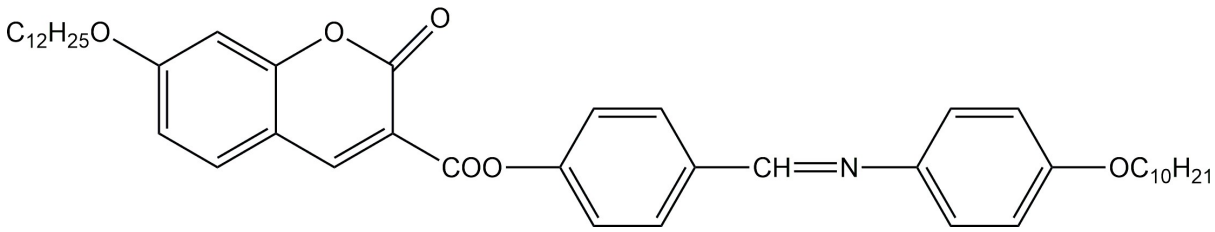

Light yellow crystal, yield 73.51%. **FT-IR** (cm^{-1}): 2965, 2920, 2855 (C-H, aliphatic), 1762 (C=O in ester), 1715 (O-C=O, cyclic ester), 1620 (C=N), 1550, 1508 (C = C, aromatic), 1248, 1218 (R-O-Ar, ether), 1014, 958, 828, 795 (C-H, aromatic). **^{1}H NMR** (400 MH_Z, $CDCl_3$) δ (ppm): 8.72 (s, 1H, Ar-H), 8.50 (s, 1H, -CH=N-), 7.95-7.57 (d, 3H, J = 8.8 Hz, Ar-H), 7.56-7.33 (d, 2H, J = 8.4 Hz, Ar-H), 6.95 (s, 1H, Ar-H), 6.94 (d, 1H, J = 2.4 Hz, Ar-H), 6.93-6.83 (d, 4H, J = 2.4 Hz, Ar-H), 4.08-4.05 (t, 4H,-O-CH_2-), 1.89-1.29 (m, 36H, -CH_2-CH_2-), 0.92-0.88 (t, 6H, -CH_2-CH_3). **^{13}C NMR** (150 MHz, $CDCl_3$) δ (ppm): 165.4 (-C=O), 161.8 (-CH=N-), 144.3 (-C-N), 158.3, 158.3, 156.8, 150.4, 131.3, 130.8, 130.7, 129.8, 122.4, 122.5, 115.1, 115.0, 114.8, 114.4, 100.8 (Ar-C), 69.1, 68.3 (Ar-O-CH_2-), 31.9, 31.9, 31.8, 31.8, 30.9, 30.7, 30.5, 29.5, 29.4, 29.3, 29.2, 29.1, 29.0, 28.9, 28.8, 28.8, 28.7, 26.0, 25.9, 25.8 (-CH_2-CH_2-), 22.6 (-CH_2-CH_3), 14.1 (-CH_2-CH_3).

4'-(4''-n-decyloxyphenyl iminomethyl)phenyl, 7-n-tetradecyloxy-2-oxo-4[*H*]-chromene-3-carboxylate (6l)

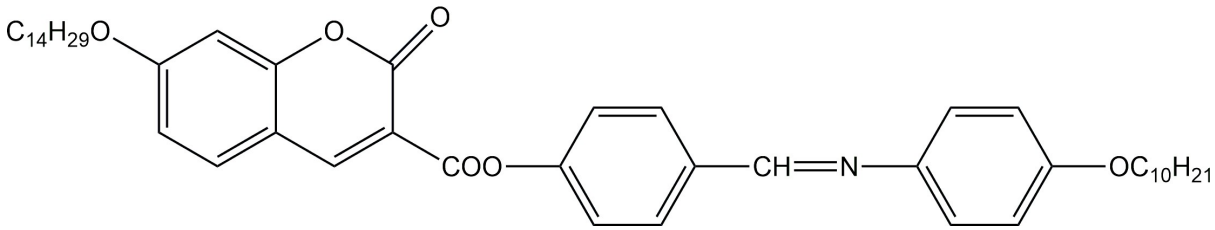

Yellow crystal, yield 73.33%. **FT-IR** (cm^{-1}): 2953, 2920, 2850 (C-H, aliphatic), 1764 (C=O in ester), 1718 (O-C=O, cyclic ester), 1618 (C=N), 1506 (C = C, aromatic), 1246, 1217 (R-O-Ar, ether), 1013, 956, 827, 790 (C-H, aromatic). **^{1}H NMR** (400 MHz, $CDCl_3$) δ (ppm): 8.74 (s, 1H, Ar-H), 8.51 (s, 1H, -CH=N-), 7.97-7.58 (d, 3H, J = 8.4 Hz, Ar-H), 7.57-7.35 (d, 2H, J = 8.8 Hz, Ar-H), 6.94 (s, 1H, Ar-H), 6.96 (d, 1H, J = 2.4 Hz, Ar-H), 6.95-6.83 (d, 4H, J = 2.4 Hz, Ar-H), 4.08-4.01 (t, 4H,-O-CH_2-), 1.89-1.29 (m, 40H, -CH_2-CH_2-), 0.92-0.88 (t, 6H, -CH_2-CH_3). **^{13}C NMR** (150 MHz, $CDCl_3$) δ (ppm): 165.5 (-C=O), 161.6 (-CH=N-), 144.5 (-C-N), 158.0, 158.0, 156.9, 152.6, 150.5, 134.4, 131.0, 130.9, 129.7, 122.2, 122.0, 115.0, 114.8, 114.6, 114.3, 112.5, 111.4, 100.8, 100.7 (Ar-C), 69.1, 68.3 (Ar-O-CH_2-), 31.9, 31.9, 29.6, 29.6, 29.5, 29.5 , 29.4, 29.3, 29.3, 28.8, 26.0, 25.9 (-CH_2-CH_2-), 22.6 (-CH_2-CH_3), 14.1 (-CH_2-CH_3).

4'-(4''-n-decyloxyphenyl iminomethyl)phenyl, 7-n-hexadecyloxy-2-oxo-4[*H*]-chromene-3-carboxylate (6m)

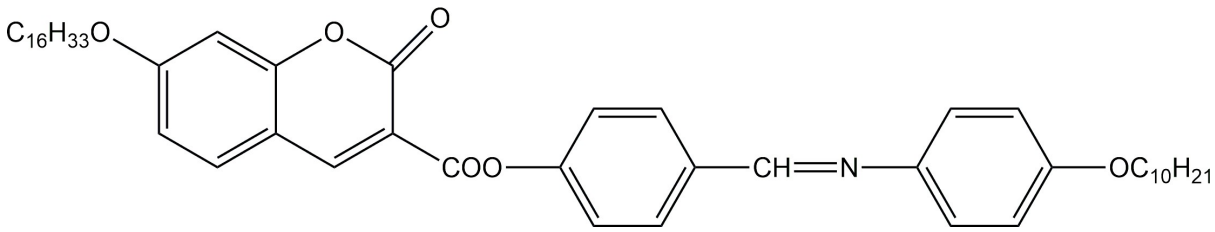

Yellow crystal, yield 74.74%. **FT-IR** (cm^{-1}): 2952, 2925, 2855 (C-H, aliphatic), 1762 (C=O in ester), 1720 (O-C=O, cyclic ester), 1620 (C=N), 1508 (C = C, aromatic), 1248, 1218 (R-O-Ar, ether), 1012, 955, 820, 788 (C-H, aromatic). **^{1}H NMR** (400 MHz, $CDCl_3$) δ (ppm): 8.71 (s, 1H, Ar-H), 8.52 (s, 1H, -CH=N-), 7.96-7.58 (d, 3H, J = 8.8 Hz, Ar-H), 7.57-7.34 (d, 2H, J = 8.4 Hz, Ar-H), 6.96 (s, 1H, Ar-H), 6.95 (d, 1H, J = 2.4 Hz, Ar-H), 6.95-6.83 (d, 4H, J = 2.4 Hz, Ar-H), 4.08-4.01 (t, 4H,-O-CH_2-), 1.89-1.29 (m, 44H, -CH_2-CH_2-), 0.92-0.88 (t, 6H, -CH_2-CH_3). **^{13}C NMR** (150 MHz, $CDCl_3$) δ (ppm): 165.4 (-C=O), 161.8 (-CH=N-), 144.3 (-C-N), 158.3, 158.3, 156.8, 150.4, 131.3, 130.8, 130.7, 129.8, 122.4, 122.5, 115.1, 115.0, 114.8, 114.4,

100.8 (Ar-C), 69.1, 68.3 (Ar-O-CH_2-), 31.9, 31.9, 31.8, 31.8, 30.9, 30.7, 30.5, 29.5, 29.4, 29.3, 29.2, 29.1, 29.0, 28.9, 28.8, 28.8, 28.7, 26.0, 25.9, 25.8 (-CH_2-CH_2-), 22.6 (-$\underline{C}H_2$-CH_3), 14.1 (-CH_2-$\underline{C}H_3$).

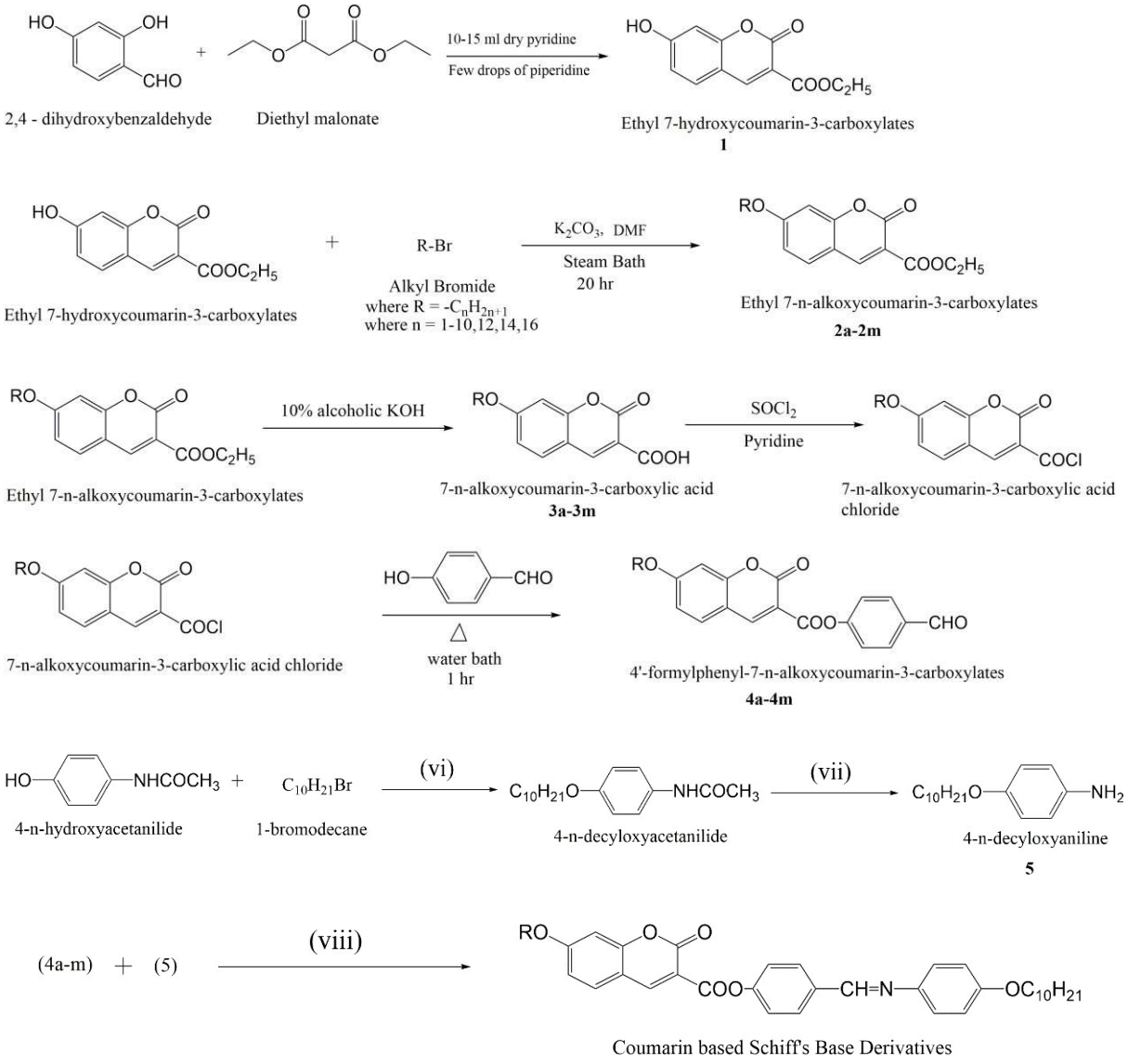

Series-I (6a-6m);

R = -C_nH_{2n+1} and n = 1-10,12,14,16

Scheme 3.1: The synthetic strateg of Series-I (**6a-6m)**. Reagents and conditions: (i) dry pyridine, few drops of piperidine (ii) K_2CO_3, DMF, steam bath 20 h (iii) 10% alcoholic KOH (iv) $SOCl_2$, pyridine (v) p-hydroxybenzaldehyde, pyridine, heat on water bath 1 h (vi) anhydrous K_2CO_3, dry acetone, reflux 8-10 h, 70-80 °C (vii) hydrolysis in presence of acid (viii) absolute EtOH, few drops of glacial AcOH, reflux 3-4 h

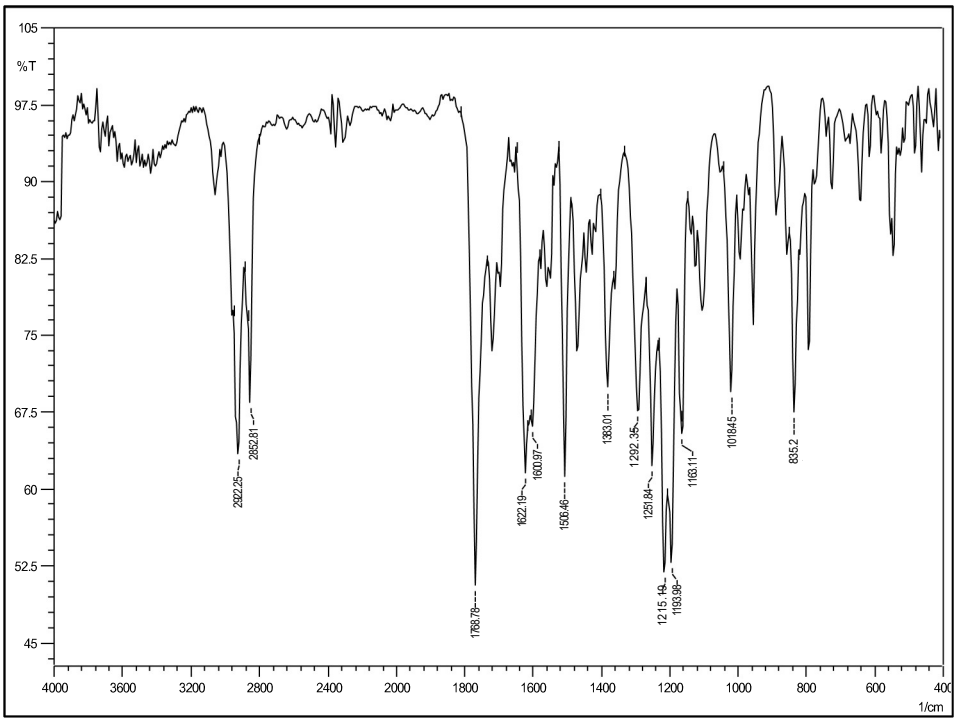

Figure 3.4: FT-IR spectra of 4’-(4’’-n-decyloxyphenyl iminomethyl)phenyl, 7-n-methoxy-2-oxo-4[*H*]-chromene-3-carboxylate (6a)

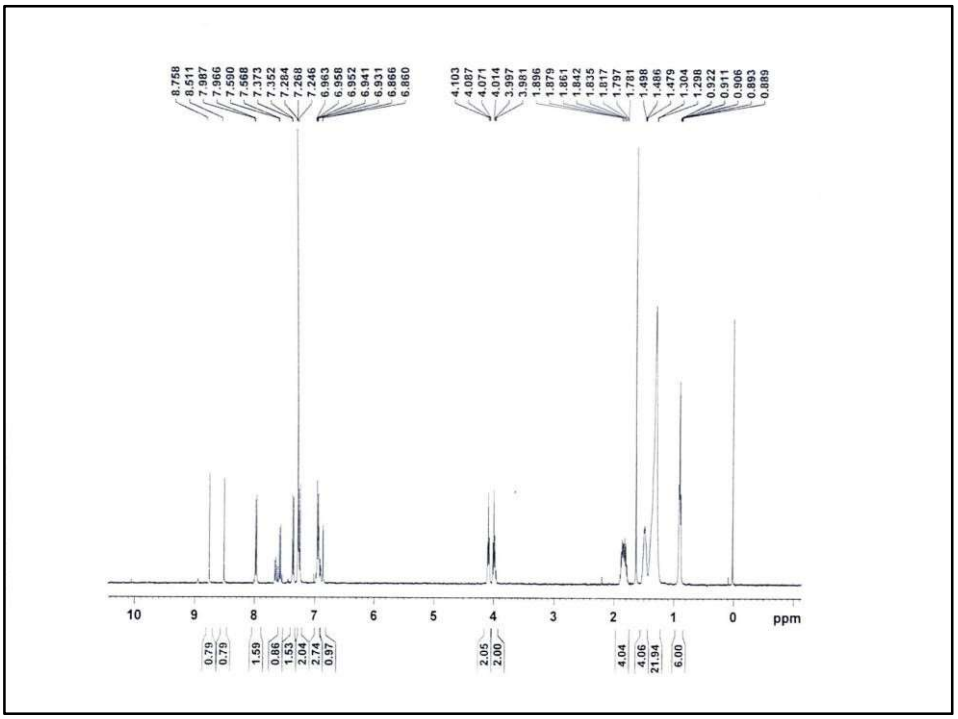

Figure 3.5: ^{1}H NMR spectra of 4’-(4’’-n-decyloxyphenyl iminomethyl)phenyl, 7-n-methoxy-2-oxo-4[*H*]-chromene-3-carboxylate (6a)

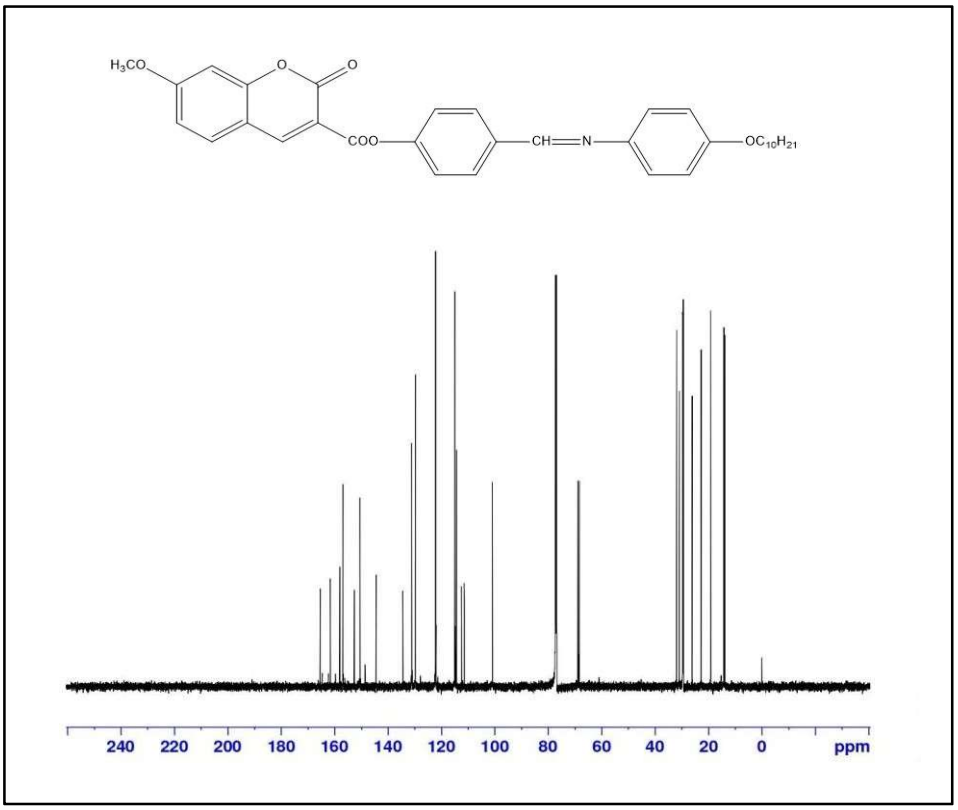

Figure 3.6: ^{13}C NMR spectra of 4'-(4''-n-decyloxyphenyl iminomethyl)phenyl, 7-n-methoxy-2-oxo-4[*H*]-chromene-3-carboxylate (6a)

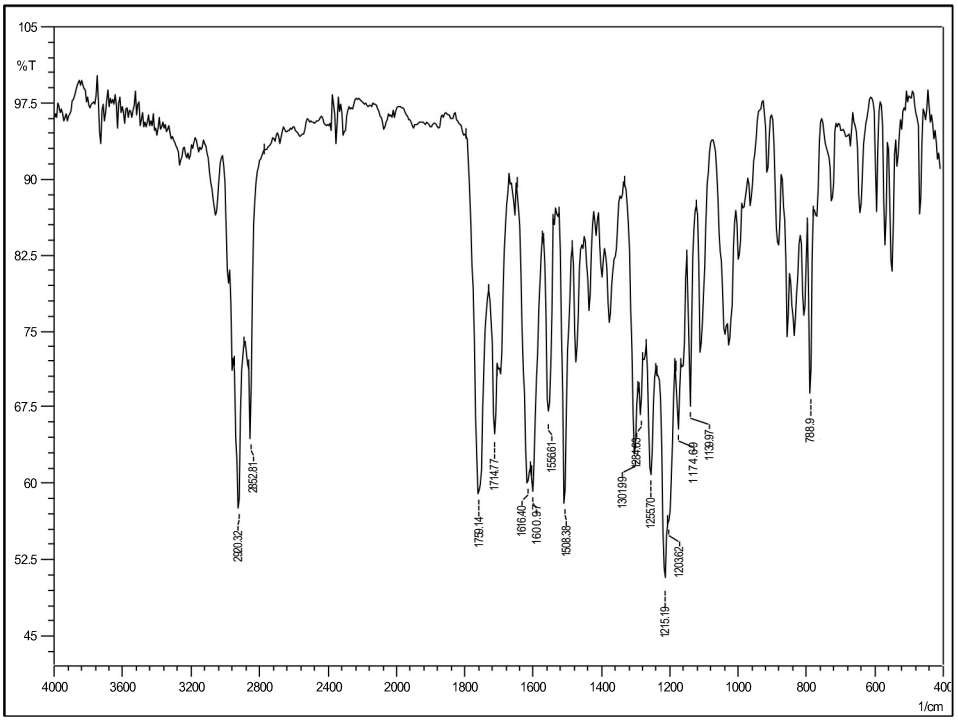

Figure 3.7: FT-IR spectra of 4'-(4''-n-decyloxyphenyl iminomethyl)phenyl, 7-n-ethoxy-2-oxo-4[*H*]-chromene-3-carboxylate (6b)

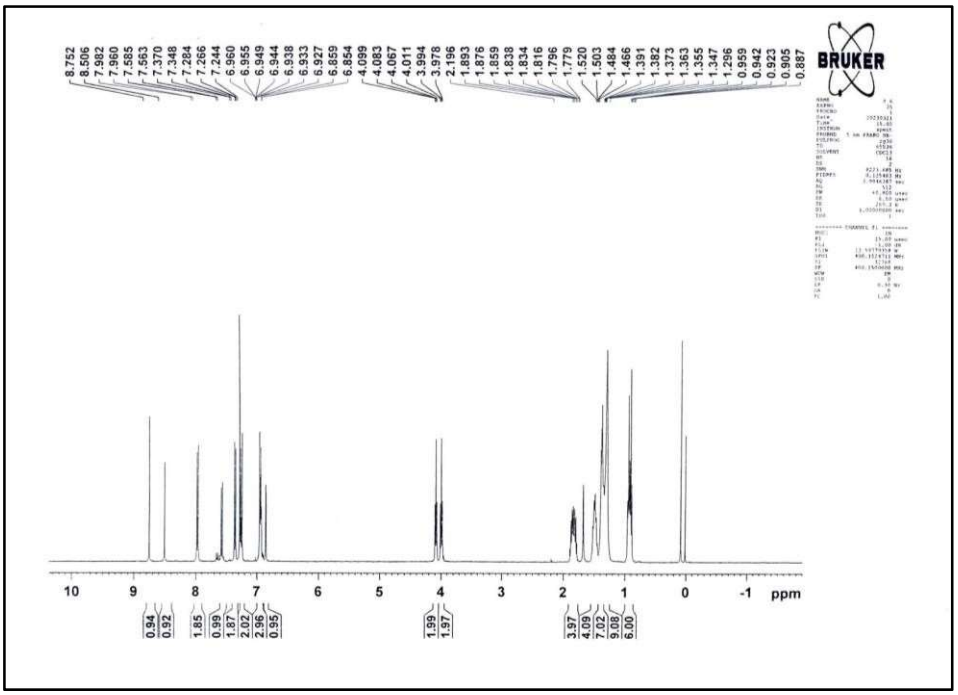

Figure 3.8: ^{1}H NMR spectra of 4'-(4''-n-decyloxyphenyl iminomethyl)phenyl, 7-n ethoxy-2-oxo-4[*H*]-chromene-3-carboxylate (6b)

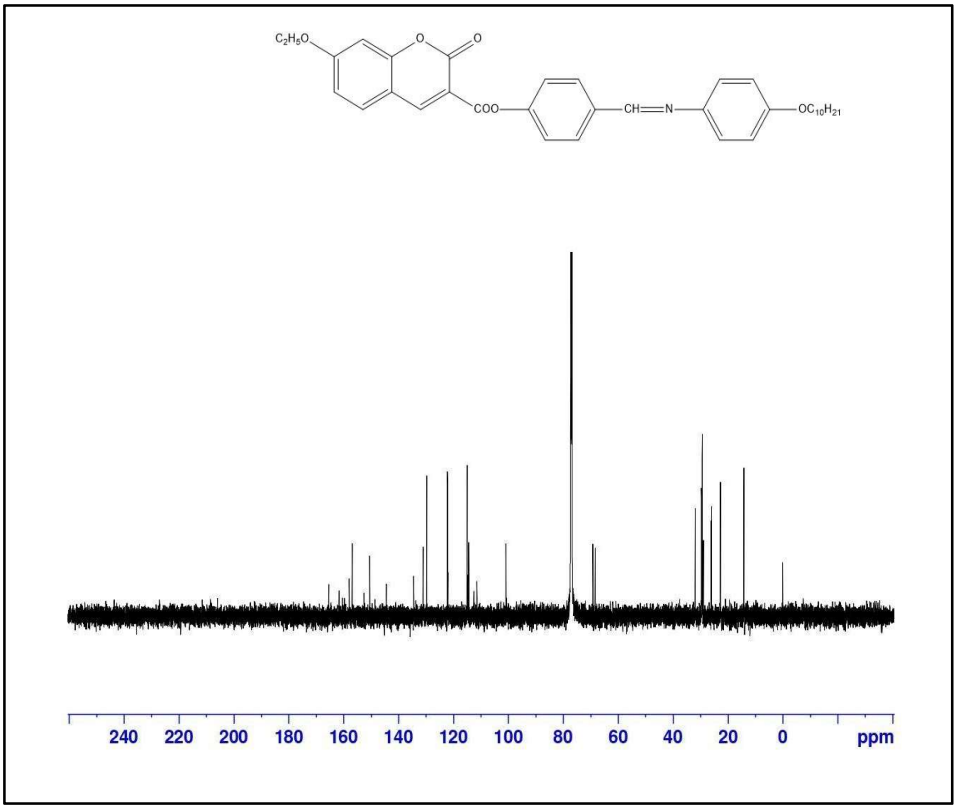

Figure 3.9: ^{13}C NMR spectra of 4'-(4''-n-decyloxyphenyl iminomethyl)phenyl, 7-n-ethoxy-2-oxo-4[*H*]-chromene-3-carboxylate (6b)

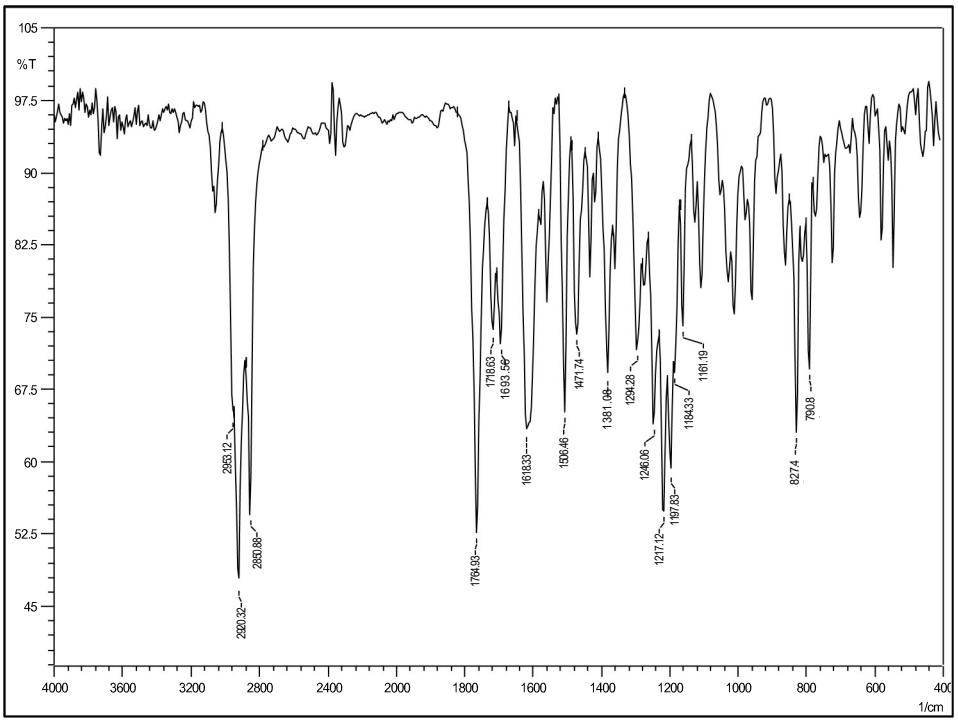

Figure 3.10: FT-IR spectra of 4'-(4''-n-decyloxyphenyliminomethyl)phenyl,7-n-tetradecyloxy-2-oxo-4[*H*]-chromene-3-carboxylate (6l)

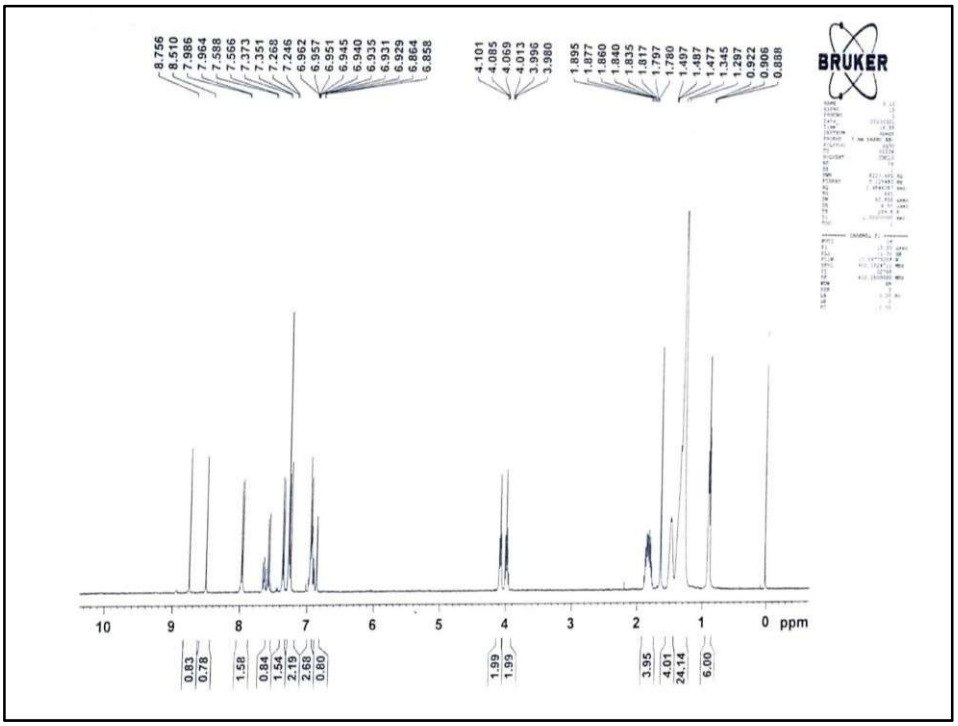

Figure 3.11: ^{1}H NMR spectra of 4'-(4''-n-decyloxyphenyliminomethyl)phenyl,7-n-tetradecyloxy-2-oxo-4[*H*]-chromene-3-carboxylate (6l)

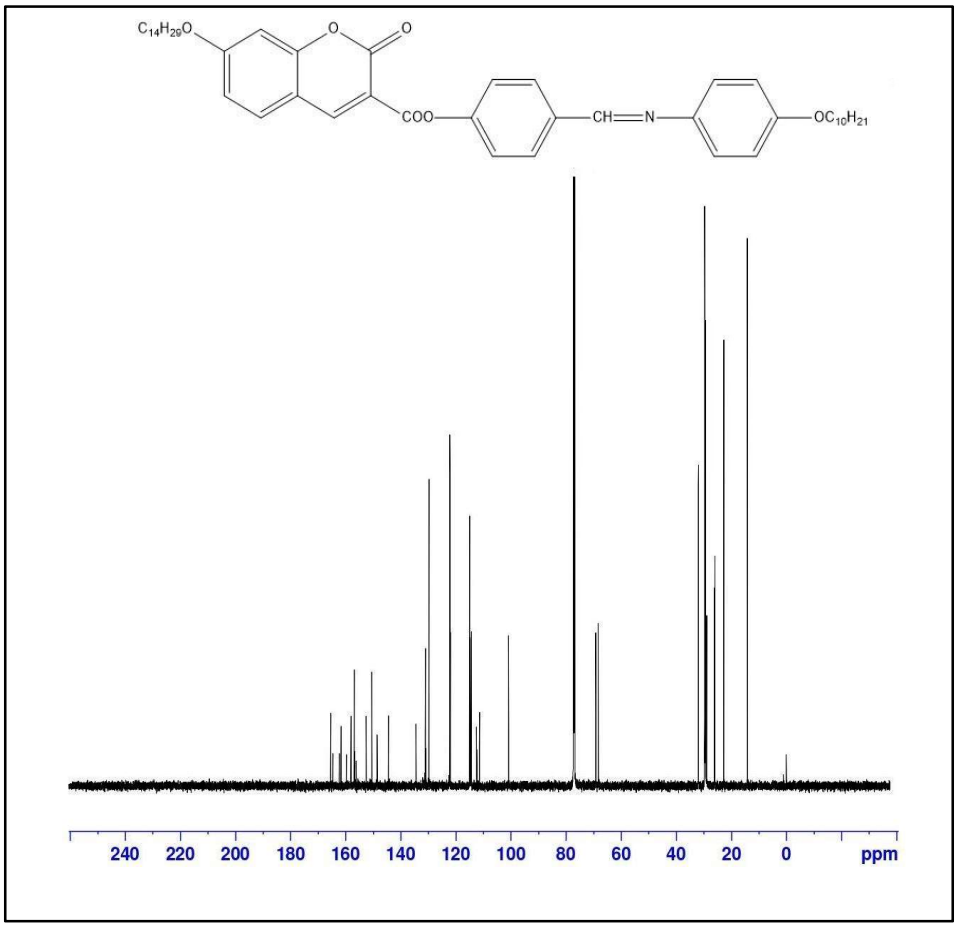

Figure 3.12: ^{13}C NMR spectra of 4'-(4''-n-decyloxyphenyl iminomethyl)phenyl, 7-n-tetradecyloxy-2-oxo-4[*H*]-chromene-3-carboxylate (6l)

Table 3.1: Physical data of Series-I (6a-6m)

Compound code	n	Mol. Formula	% Yield	Elemental Analysis					
				Calculated			Found		
				C	H	N	C	H	N
6a	1	$C_{34}H_{37}NO_6$	73.12	73.49	6.71	2.52	73.45	6.69	2.49
6b	2	$C_{35}H_{39}NO_6$	75.11	73.79	6.90	2.46	73.73	6.88	2.43
6c	3	$C_{36}H_{41}NO_6$	76.58	74.08	7.08	2.40	74.02	7.04	2.38
6d	4	$C_{37}H_{43}NO_6$	76.15	74.35	7.25	2.34	74.30	7.22	2.32
6e	5	$C_{38}H_{45}NO_6$	75.10	74.61	7.41	2.29	74.55	7.38	2.26
6f	6	$C_{39}H_{47}NO_6$	73.48	74.85	7.57	2.24	74.80	7.55	2.20
6g	7	$C_{40}H_{49}NO_6$	78.50	75.09	7.72	2.19	75.02	7.70	2.16
6h	8	$C_{41}H_{51}NO_6$	78.06	75.31	7.86	2.14	75.25	7.83	2.11
6i	9	$C_{42}H_{53}NO_6$	79.51	75.53	8.00	2.10	75.45	7.98	2.08
6j	10	$C_{43}H_{55}NO_6$	72.73	75.74	8.13	2.05	75.68	8.12	2.03
6k	12	$C_{45}H_{59}NO_6$	73.51	76.13	8.38	1.97	76.05	8.35	1.95
6l	14	$C_{47}H_{63}NO_6$	73.33	76.49	8.60	1.90	76.43	8.58	1.88
6m	16	$C_{49}H_{67}NO_6$	74.74	76.83	8.82	1.83	76.78	8.80	1.81

The synthesized compounds were placed between two untreated glass slides, and observed under an optical polarising microscope, measurements of the transition temperatures and microscopic textures were made during both cycles to ascertain the compound's mesomorphic character. Series-I exhibit an enantiotropic nematic phase.

3.3. Results and Discussion

The proposed final compounds were prepared by condensation of 4-n-decyloxyaniline with 4'-formylphenyl-7-n-alkoxycoumarin-3-carboxylates. Nematic phases were observed in the prepared compounds. The fluorescence data of all the synthesized compounds **(6a-6m)** are depicted in Table 3.2. Different enthalpy change values for Cr-N and N-I transition temperatures were noted in Table 3.4. The molecular shape of the compound which imparts bending in the molecule is responsible for the enthalpy change observed in N-I transitions.

3.3.1 Photophysical studies, and TGA

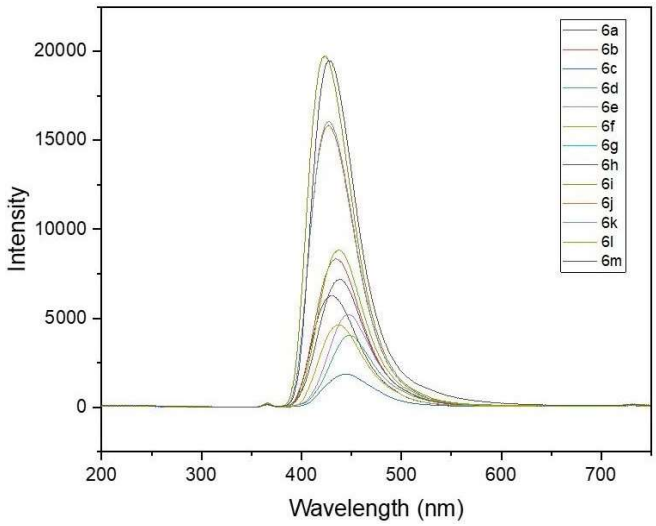

Figure 3.13: Fluorescence spectra of the compounds **6a-6m** excited at 365 nm.

The fluorescence emission spectra of the compounds **6a-6m** were examined in the mixture of ethanol and chloroform (60:40). It was found that all the prepared compounds exhibit fluorescence on excitation at 365 nm. It was observed that the final prepared coumarin-based Schiff's base derivatives exhibit fluorescence ranging wavelength between 424-448 nm. 4-n-alkoxy group at the terminal end and a coumarin moiety are responsible for the intramolecular charge transfer (ICT) in the same direction. The incorporation of the ester group and Schiff's base in the coumarin moiety influences ICT and results in a fluorescence emission spectrum. The observed fluorescence spectra (of compounds 6a-6m) are similar as observed earlier on the incorporation of the ester and the imine group in the moiety [61]. With the gradual increase in –OR group, besides coumarin moiety, fluorescence intensity increases continuously. However, a lower chain length shows a red shift in the emission peak, and a higher chain length causes a blue shift. Further, the medium alkoxy chain length shows a constancy in the λmax. Generally, fluorescence behavior is governed by chain length, л-л stacking, and molecular rigidity among others. A longer hydrocarbon chain in an alkoxy group can result in a nearer arrangement of molecules, improving л-л stacking between neighboring fluorescence groups. This may contribute to enhance the energy transfer together with enhanced fluorescence intensity. However, this effect was prominent with higher chain-length mesogenic materials. This effect cannot be true for the lower alkoxy chain length group attached to the coumarin

moiety. This is because such compounds may behave flexibly resulting in redshift. The above behavior can be seen from the perusal of Figure 3.13.

Table 3.2: Fluorescence data of all the synthesized compounds

Compound Code	R= $-C_nH_{2n+1}$ n	Wavelength λmax.(nm)
6a	1	430
6b	2	434
6c	3	443
6d	4	447
6e	5	447
6f	6	436
6g	7	423
6h	8	438
6i	9	423
6j	10	427
6k	12	427
6l	14	436
6m	16	427

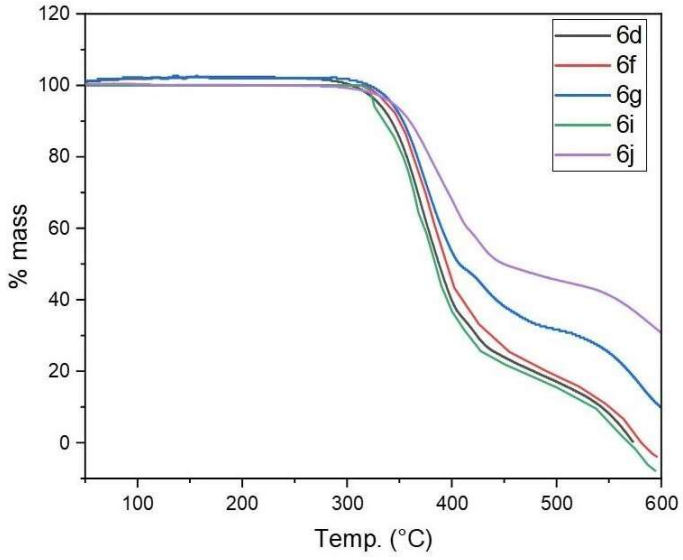

Figure 3.14: Representative TGA thermogram of compounds **6d**, **6f**, **6g**, **6i**, and **6j** was recorded under nitrogen atmosphere.

The TGA measurements of the compounds **6d, 6f, 6g, 6i,** and **6j** were performed in a temperature range from 50-600 °C in a nitrogen atmosphere. It was observed that there is no weight loss up to 300 °C which indicates the thermal stability of final synthesized compounds (Figure 3.14).

3.3.2 Mesomorphic properties of compounds (6a-6m) of Series-I

Liquid crystalline property of all the final compounds were examined under POM and their transition temperatures were compared using DSC. Schlieren nematic texture with four brush in compound **6d** has been presented in Figure 3.15 (c). In Figure 3.15 (c), four brush defect confirms the presence of nematic ordering [72].

In general, a mesogen's isotropic temperature may vary depending on the length of the hydrocarbon chain. Therefore, a compound's melting point would increase as its chain length increased due to an increase in van der Waals interactions. Conversely, the hydrocarbon chain's flexibility could affect the lateral core-core interactions, which would lower the compound's isotropic temperature. Due to the higher isotropic temperature in the synthesized homologous series of coumarin derivatives, the packing arrangement and linearity of the molecules may be affected, due to which the $T_{I\text{-}N}$ temperatures (in the cooling cycle) are found lower than the $T_{N\text{-}I}$ temperatures (in the heating cycle) [73].

The dimensionless quantity $\Delta S_{N\text{-}I}/R$ represents the dependency of the entropy change linked to the nematic–isotropic transition. It was observed that the value of $T_{N\text{-}I}$ and $\Delta S_{N\text{-}I}/R$ may depend upon the variance in length and parity of the spacer molecules in the synthesized moiety. From the data represented in Table 3.4, it is noted that the dependence of the entropy change value is altered dramatically as the n increases in the synthesized compounds. This increases the nematic phase's orientational order, resulting in a higher value of $\Delta S_{N\text{-}I}/R$ than would be predicted for a typical low liquid crystal made up of a single mesogenic unit. In contrast, the orientational order of the nematic phase cannot drive the interconversion of conformers because the difference in free energy between the bent and linear forms is too higher. As a result, a smaller $\Delta S_{N\text{-}I}/R$ would be expected [74-76].

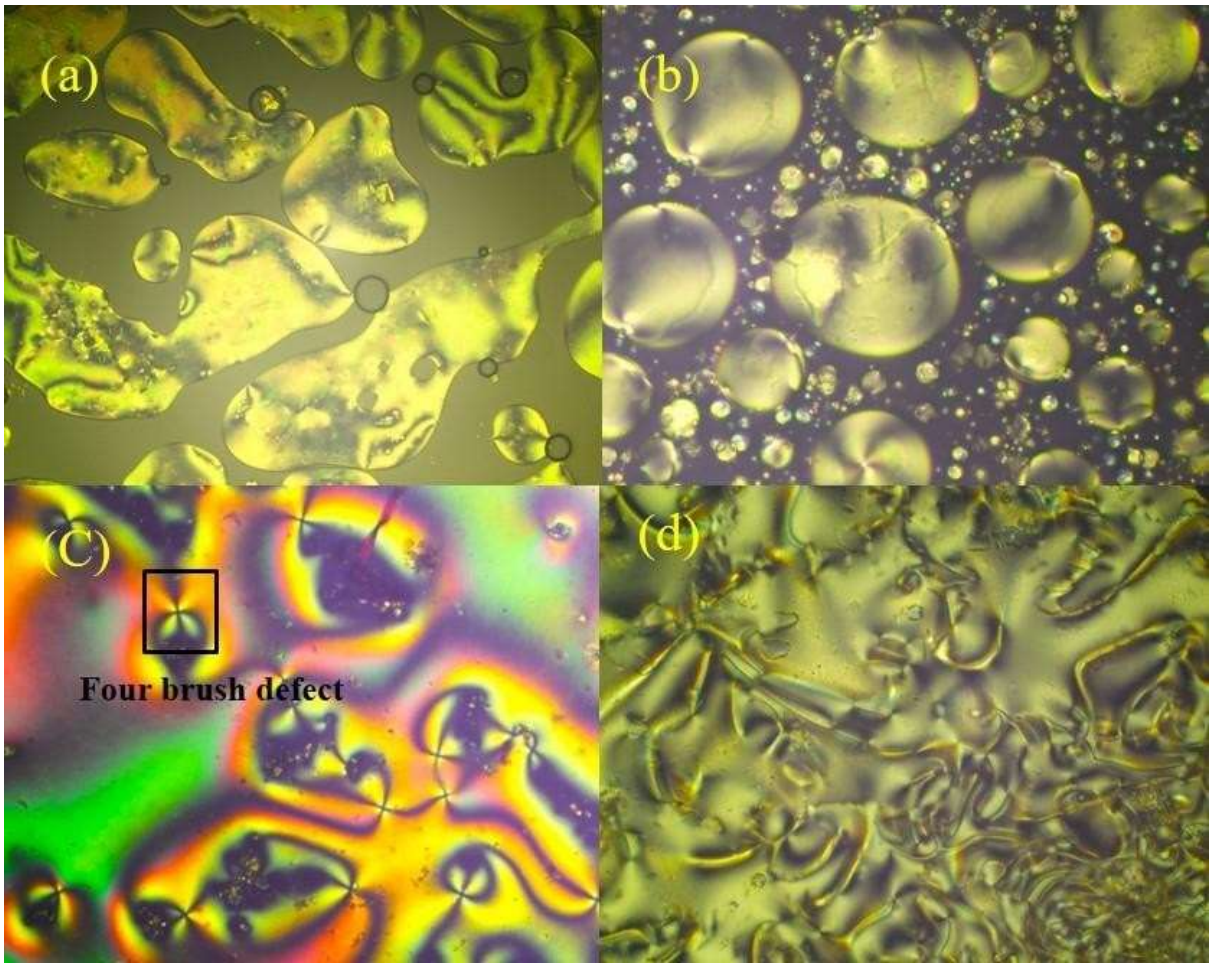

Figure 3.15: POM textures of coumarin based Schiff's-base derivatives upon heating and cooling cycles using untreated microscopic glass slides: (a) Compound **6b** nematic phase observed at 286.3 °C on cooling (b) Compound **6e** nematic phase with typical marble texture observed at 268.4 °C on cooling (c) Compound **6d** Schlieren nematic texture observed at 270.1 °C on heating (d) Compound **6c** thread like nematic texture observed at 275.1 °C on heating. All the microscopic textures were taken under the magnification of 10 X.

Table 3.3: Transition temperatures of Series-I (6a-6m) recorded in polarizing optical microscope.

Sr. No.	Comp. Code	R = *n*-alkyl group	Transition temperatures (°C)				
			Cr		N*		I
1	6a	Methyl	•	294.2	•	304.4	•
2	6b	Ethyl	•	289.1	•	298.0	•
3	6c	Propyl	•	274.1	•	288.5	•
4	6d	Butyl	•	269.5	•	290.5	•
5	6e	Pentyl	•	273.5	•	286.1	•
6	6f	Hexyl	•	276.9	•	287.5	•
7	6g	Heptyl	•	267.1	•	288.1	•
8	6h	Octyl	•	265.4	•	289.4	•
9	6i	Decyl	•	262.4	•	281.1	•
10	6j	Dodecyl	•	258.1	•	268.1	•
11	6k	Tetradecyl	•	258.8	•	268.8	•
12	6l	Hexadecyl	•	257.1	•	269.1	•
13	6m	Octadecyl	•	258.5	•	268.5	•

Cr = crystal, N* = nematic, I = isotropic.

Table 3.4: Phase transition temperatures of Series-I compounds (6a-6m)a upon heating and cooling.

Compound code	n-alkyl group	Transition temperatures(°C)		$\Delta S_{CrN}/R$ Heating	$\Delta S_{NI}/R$ Heating	$\Delta S_{IN}/R$ Cooling	$\Delta S_{NCr}/R$ Cooling
		Heating Temp.°C[ΔH kJ mol^{-1}]	Cooling Temp.°C[ΔH kJ mol^{-1}]				
6a	1	Cr 295.1[11.90] N 305.2[0.45] I	I 294.1[0.39] N 100.4[11.10] Cr	20.94	0.77	0.68	29.72
6b	2	Cr 290.2[10.10] N 299[0.88] I	I 286.3[0.65] N 99.1[9.56] Cr	17.93	1.53	1.16	25.69
6c	3	Cr 275.1[8.80] N 290.3[0.90] I	I 271.4[0.82] N 109.3[8.25] Cr	16.05	1.59	1.50	21.57
6d	4	Cr 270.1[9.90] N 289.1[0.35] I	I 265.1[0.32] N 91.1[9.10] Cr	18.22	0.62	0.59	24.99
6e	5	Cr 275.1[9.80] N 287.2[0.40] I	I 268.4[0.35] N 100.4[8.90] Cr	17.87	0.71	0.64	23.83
6f	6	Cr 278.8[8.85] N 286.1[0.10] I	I 270.1[0.08] N 105.4[8.10] Cr	16.03	0.17	0.14	21.40
6g	7	Cr 268.2[6.60] N 287.1[0.20] I	I 260.2[0.15] N 101.3[6.10] Cr	12.19	0.35	0.28	16.29
6h	8	Cr 266.4[7.80] N 288.5[0.11] I	I 262.3[0.09] N 130.1[7.21] Cr	14.46	0.19	0.16	17.88
6i	9	Cr 263.4[8.81] N 280.3[0.06] I	I 261.3[0.05] N 123.2[8.10] Cr	16.42	0.10	0.09	20.44
6j	10	Cr 260.5[8.21] N 270.4[0.10] I	I 256.2[0.08] N 120.3[7.65] Cr	15.38	0.18	0.15	19.45
6k	12	Cr 259.6[7.95] N 269.1[0.25] I	I 255.1[0.20] N 122.3[7.10] Cr	14.92	0.46	0.37	17.96
6l	14	Cr 258.6[6.50] N 268.8[0.10] I	I 252.2[0.07] N 125.6[6.01] Cr	12.27	0.18	0.13	15.07
6m	16	Cr 257.3[7.50] N 267.4[0.30] I	I 253.2[0.25] N 126.4[6.91] Cr	14.14	0.55	0.47	17.30

Cr-crystalline solid, N-nematic mesophase, I-isotropic liquid

[a]Phase transition temperatures were noted by Differential Scanning Calorimetry studies: peak temperatures in the DSC thermograms obtained during the first heating and cooling cycles (scanning rate = 5 °C min^{-1}).

3.3.3 DSC of compounds 6a, 6e, and 6h

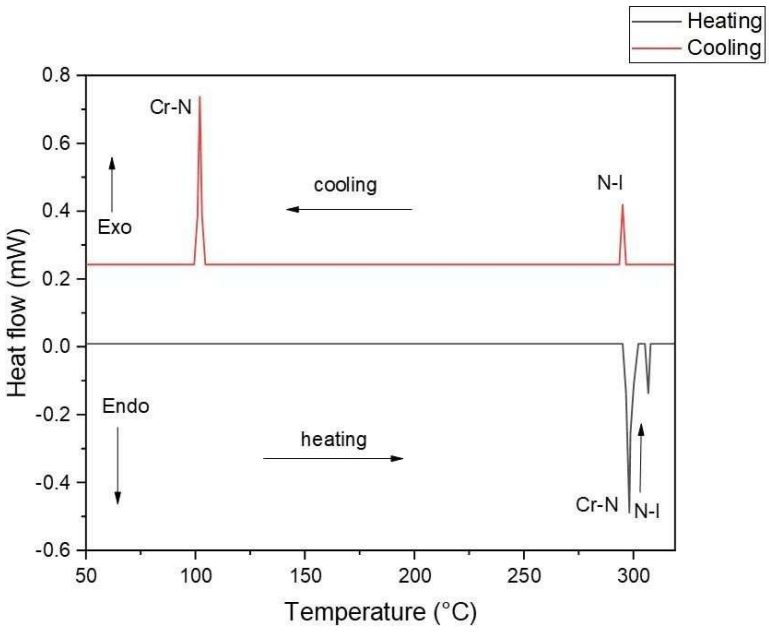

DSC of compound 6a

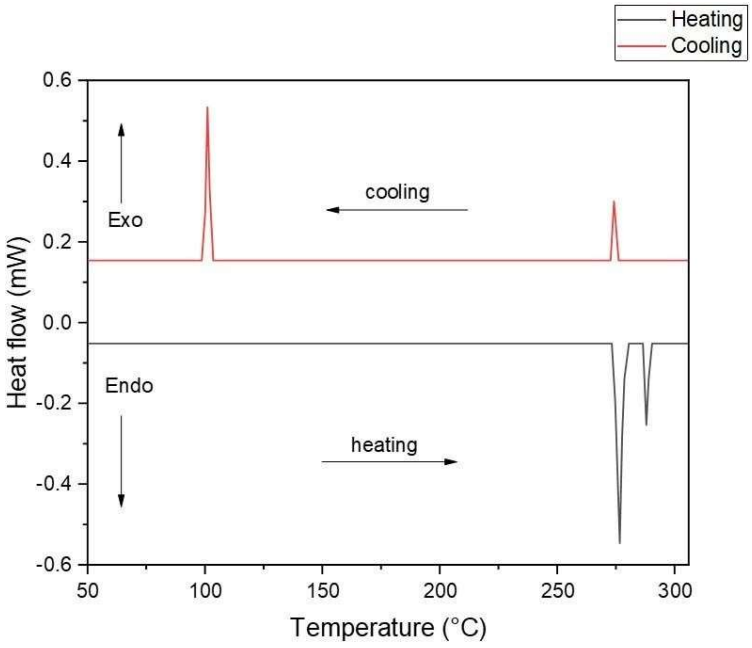

DSC of compound 6e

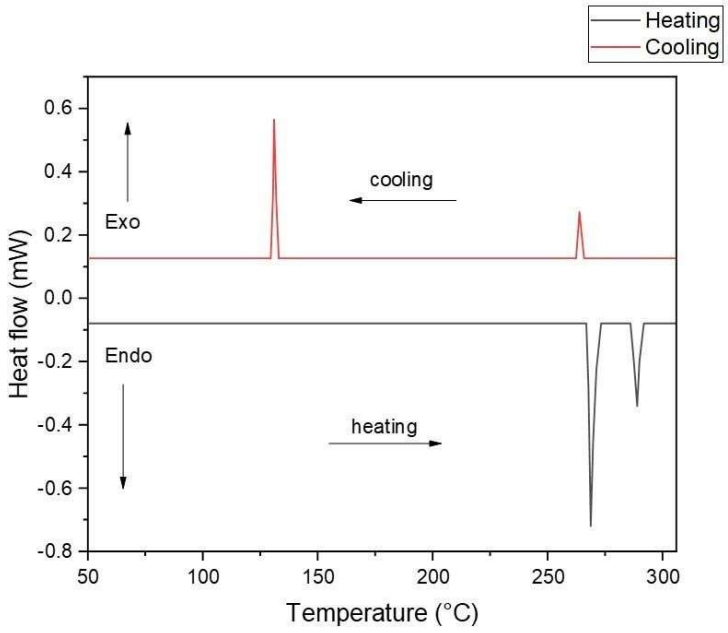

DSC of compound 6h

Figure 3.16: DSC of representative compounds 6a, 6e, and 6h.

3.3.4 DFT Calculations and mesomorphic comparison

DFT study was carried out for the representative synthesized compounds **6d**, **6e**, **6g**, **6h**, **6k** respectively. Using the DFT/B3LYP approach, Orca 5.0 [Functional - B3LYP, Basis set - def-TZVP, RIJCOSX] software performed all of the theoretical computations for the synthesized substances. To create a novel minimum-energy geometrical structure, the geometrical structures of compounds were optimized by minimizing the energy of conformations with respect to all geometrical parameters. Furthermore, using the same methodology and basis set, frequencies and a few thermodynamic parameters were computed using the optimized structures. Figure 3.17 displays the optimized molecular architectures.

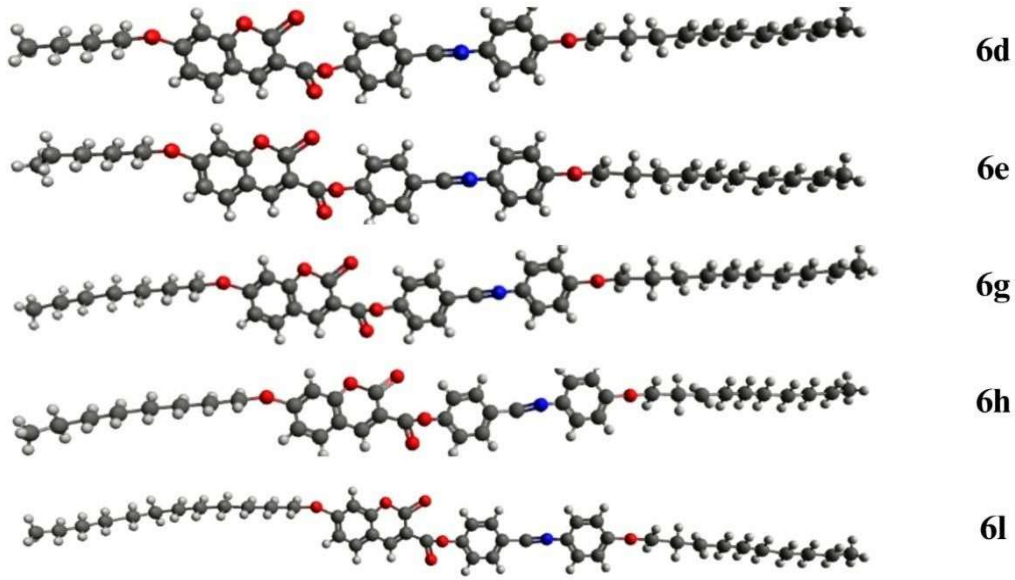

Figure 3.17: The optimised molecular geometry of the compounds **6d, 6e, 6g, 6h,** and **6l.**

The aspect ratio values, which correspond to the dimension parameters, are displayed in Table 3.5. The aspect ratio, which is the width to height ratio, can reveal the compounds collision diameter.

Table 3.5: Calculated Dimensions (A°) and aspect ratio of the investigated compounds.

Compound Code	Length (L)	Width (D)	Aspect Ratio (L/D)
6d	31.57	11.25	2.80
6e	35.85	12.92	2.77
6g	40.02	13.82	2.89
6h	44.92	15.50	2.89
6k	49.51	16.00	3.09

It was expected that compounds with a high aspect ratio would exhibit higher levels of molecular packing, which would promote a more nematically organized mesophase. As the number of carbons in the terminal alkyl chains increases, the variance in the aspect ratio trend in the synthesized compounds (**6d, 6e, 6g, 6h, and 6k**) was found. This is because, when the

terminal alkyl compounds (**6d, 6e, 6g, 6h, and 6k**) develop diagonally in the space, their breadth increases, and their aspect ratio values fall.

Table 3.6: Frontier molecular orbitals energies (eV) of 6d, 6e, 6g, 6h, and 6k compounds.

Compound code	ELUMO	EHOMO	ΔE
6d	-3.278	-3.404	0.126
6e	-3.257	-3.385	0.128
6g	-3.180	-3.308	0.128
6h	-3.192	-3.319	0.127
6k	-3.085	-3.212	0.127

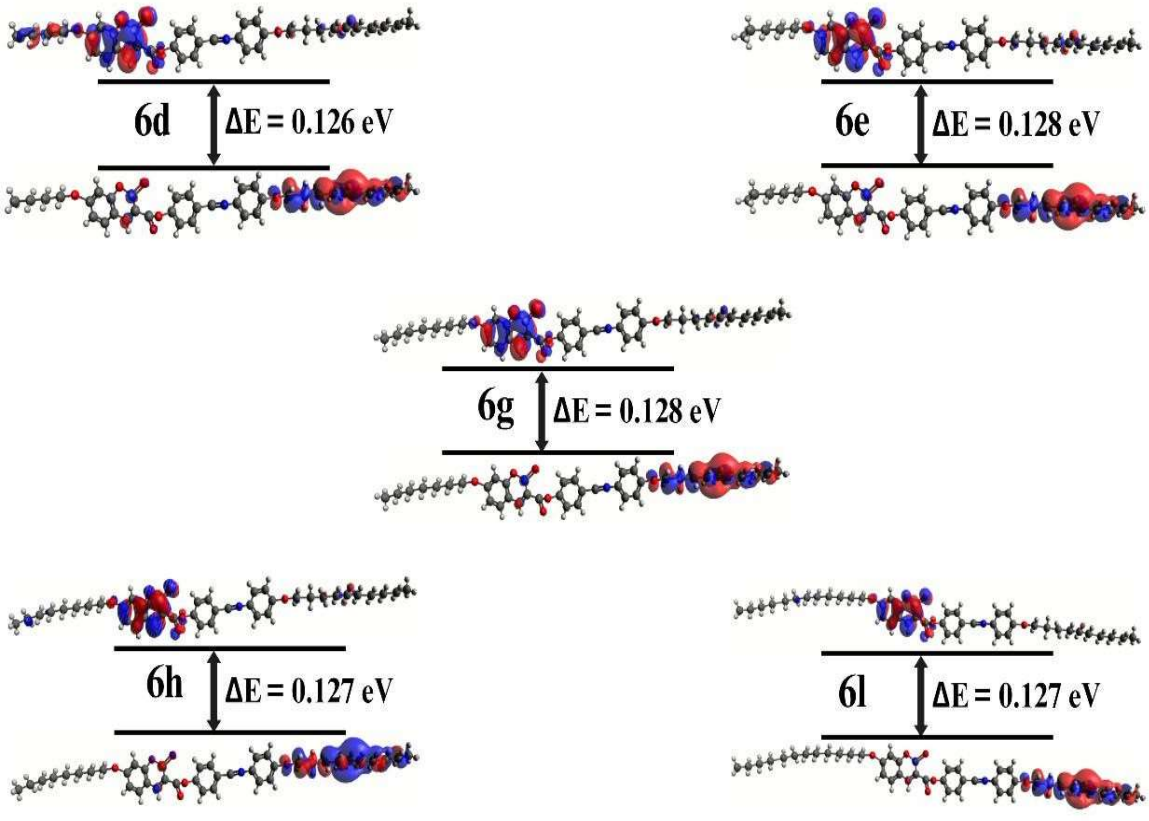

Figure 3.18: The estimated Frontier molecular orbitals of compounds **6d, 6e, 6g, 6h,** and **6k**.

3.3.5 Frontier Molecular Orbitals (FMOs)

The terms "frontier molecular orbitals" (FMOs) relate to the highest occupied (HOMO) and lowest unoccupied (LUMO) molecular orbitals. While the LUMO is an electron acceptor, the HOMO is an electron donor. The energy gap, or difference in energy between them, may be a sign of the ability for an electron to transition. Additionally, it has an inverse relationship with the molecules reactivity [73]. The compounds HOMO and LUMO orbital energies were computed using the same methodology and basis set; the outcomes are listed in Table 3.6 and shown in Figure 3.18.

The terminal chain length on both sides of the moiety has a insignificant impact on the energy gap between FMOs [74], based on the results of compounds **6d, 6e, 6g**, **6h**, and **6k**. It's important to note that this moiety has the lowest energy gap because it has an ester group (-COO-) and an azomethine group (-CH=N-), as well as an alkoxy chain length on both sides of the moiety. In addition, the difference in the energies of the FMOs is commonly used to compute a number of parameters, such as chemical hardness which is equal to $\Delta E/2$, and softness (S), which is equal to $1/\Delta E$. Since chemical hardness is the resistance to charge transference and global softness may indicate the photoelectric behaviour of liquid crystalline compounds, these two criteria can be utilised to select the proper compounds for usage in the suitable applications [75].

3.3.6 Molecular Electrostatic Potentials (MEP)

The value and vector of the dipole moment were influenced by the electron density at the atomic site of the compounds. It also affected the way molecules interacted with one another and were polarisable. The mesomorphic behaviour of liquid crystalline substances can be influenced by these characteristics For the **6d, 6e, 6g, 6h,** and **6k** compounds, the same methodologies and basis set were used to compute the molecular electrostatic potential (MEP) (Figure 3.19), which can be used as a visual method to discern the position of the electron density. Because there are more electronegative oxygen atoms in the red-colored regions, these are the sites with the most negative charge, whereas the blue-colored regions have the highest positive charge. The compounds for **6d, 6e, 6g, 6h,** and **6k** were found to have a localised negative charge in their cores. This is believed to allow for a high degree of packing, resulting in the mesomorphic behaviour of these compounds.

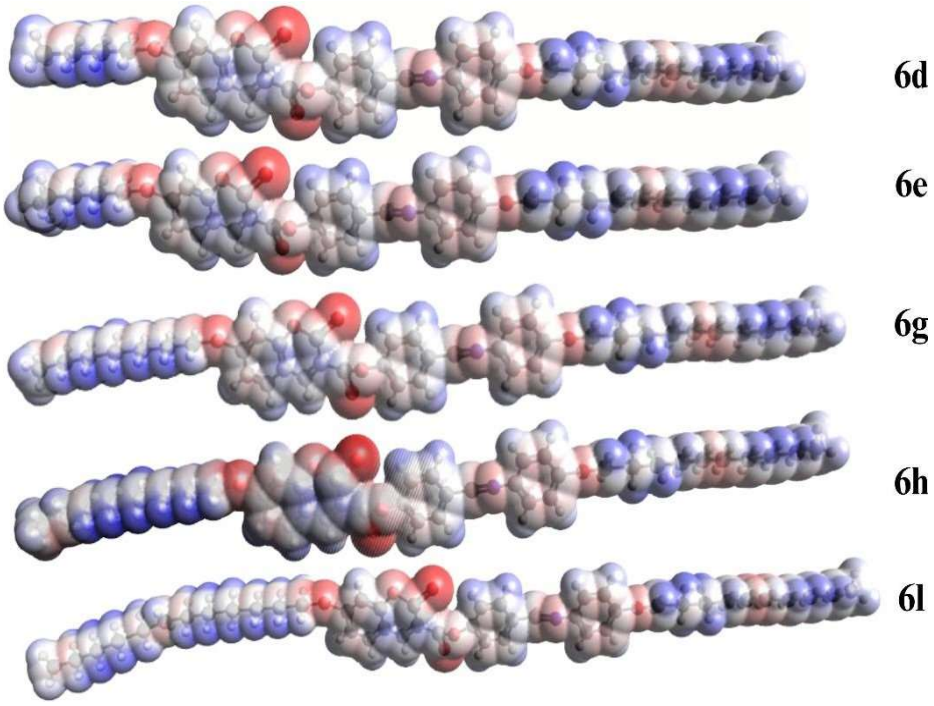

Figure 3.19: The Estimated Molecular Electrostatic Potentials (MEP) of the compounds **6d, 6e, 6g, 6h, and 6l.**

3.3.7 XRD Diffraction study

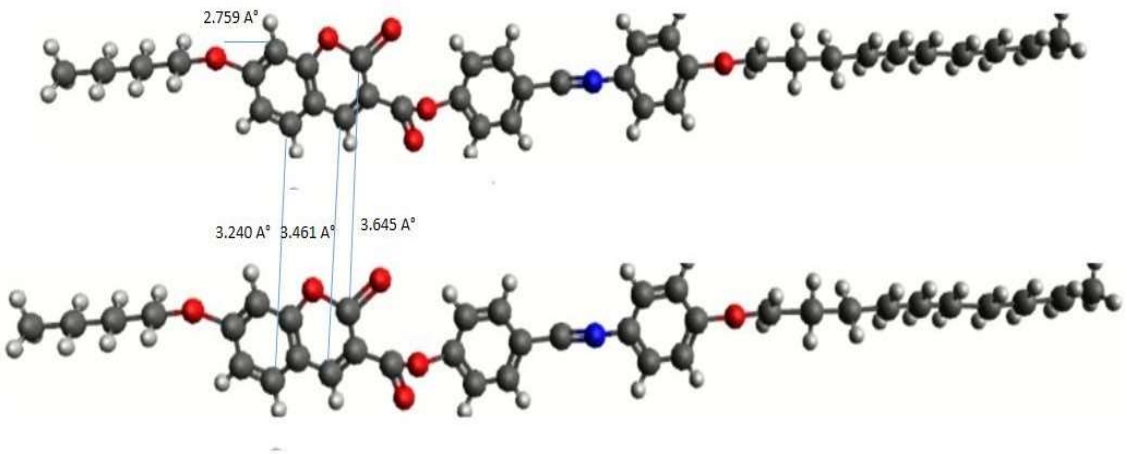

Figure 3.20: X-ray crystal analysis showing strong π···π stacking between two layers in compound **6d**.

The molecules in the unit cell were stacked one on top of the other in a linear crystal packing. As illustrated in Figure 3.20, a single molecule was found to exhibit three distinct π-π stackings: the first occurred between the phenyl rings of two distinct molecules, spaced 3.240 Å apart; the second occurred between the carbonyl carbon of lactones of two distinct molecules, spaced 3.645 Å apart; and the third occurred between the phenyl rings of coumarin moiety of two distinct molecules spaced 3.461 Å.

As seen in Figure 3.20, short connections with a value of 2.759 Å between the C-H of the benzene ring and the oxygen of the alkoxy were found in a head-to-head manner. Undoubtedly, the XRD results showed that the molecules are linear and stacked on top of one another due to intermolecular interactions [67].

3.2.1 Structure-mesomorphic property relationship

All the synthesized coumarin-based Schiff's base derivatives **6a-6m** possess enantiotropic nematic mesophases. In the series of compounds **6a-6m**, the presence of an alkyl chain at the terminal position and coumarin moiety results in high temperatures. To overcome that we have introduced an ester group in a moiety to attain low temperatures. It leads to a decrease in transition temperature while ascending the homologous series of the compound. As we ascend the series, the terminal alkyl chains restrict the packing which may lead to the formation of the nematogens [59]. Figure 3.21 depicts the transition temperature variation with number of carbon atoms present in the alkoxy chain of the mesogenic compounds. Transition temperature of the mesogenic compounds is the resultant of various factors such as molecular shape, intermolecular attractions and packing skeleton. Longer chain contributes towards flexibility of the molecule with a concomitant influence in lowering the transition temperature. Contrary to this, lower chain may results comparatively stronger intermolecular interactions with an increased transition temperature. However for a medium length alkoxy chain (n = 4-6), above two effects (flexibility and intermolecular interactions) would contribute oppositely and predominance of one over other and will decide the final transition temperatures. This indeed is observed in Figure 3.21 which indicates that balance between above mentioned factors decides the observed trends. From the graphical representation (Figure 3.21), the falling tendency in the Nematic-Isotropic transition temperature upto hexyl derivative (**6f)** was observed after that it rises with increasing methylene units till octyl derivative (**6h**) and again the falling tendency continues. In the Crystal-Nematic transition, as we ascend the series, the

falling tendency was observed till compound **6d**, after that, it rises with increasing methylene units till hexyl derivatives **6f** and again the falling tendency continues till the compound **6m.**

With increasing carbon chain length in the synthesized coumarin derivatives, smectic phases may appear but due to the higher polarizability due to the presence of alkyl chain length and the intermolecular interactions that favours directional order arrangement of molecules, only nematogenic coumarin derivatives are formed [80-82]. The irregular dependence of the N-I transition temperature is observed in Figure 3.21. This is attributed to the theory of Maier and Baumgartner which explains the alteration effect based on their study of the dipole moment and dielectric anisotropies of the nematogenic homologous series. Pines *et al*. [83] have measured the order parameters in a series of nematic liquid crystals. De Jeu and Van der Veen [84] examined a few experimental findings regarding the fluctuation of the nematic-isotropic transition temperatures (T_{N-I}) and assessed the molecular structure using molecular statistical theory expressions for T_{N-I} [85].

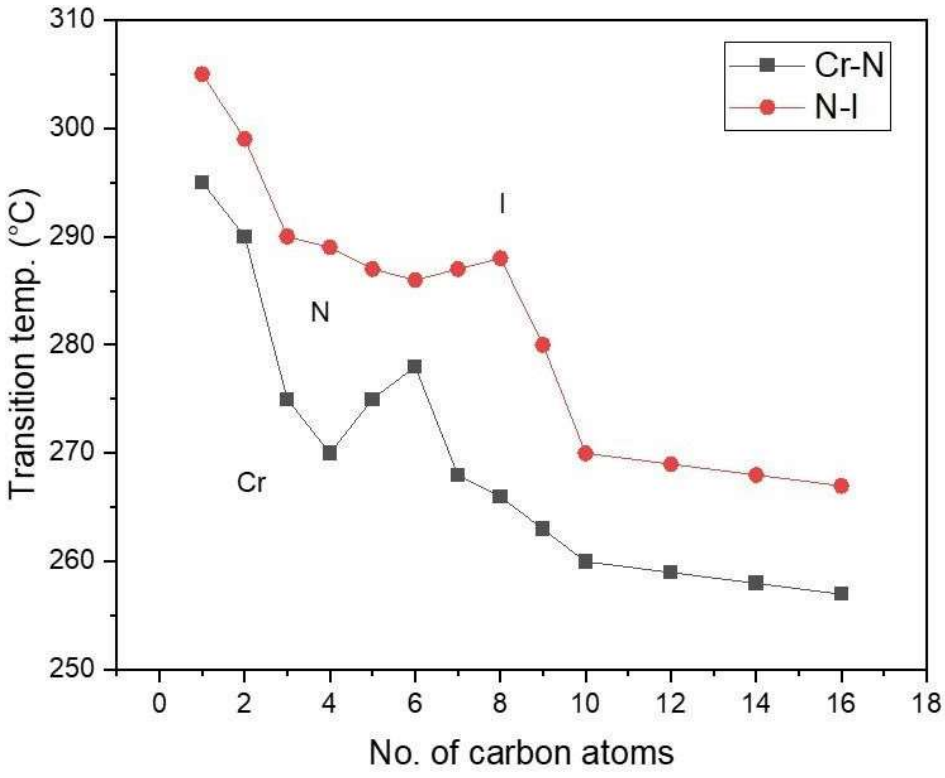

Figure 3.21: Variation of transition temperatures with a number of carbon atoms in the alkoxy chain of the mesogenic compounds.

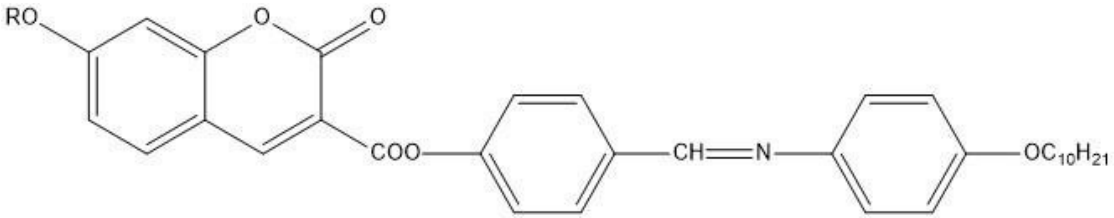

Series-I

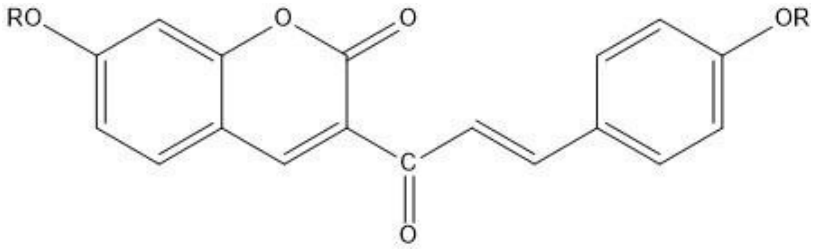

Series (A)

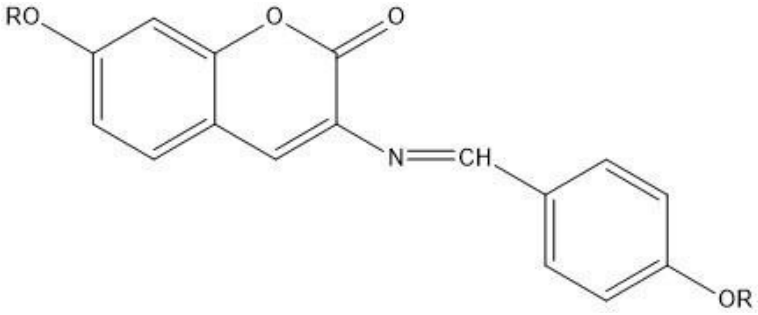

Series (B)

Figure 3.22: Structures for comparison with novel synthesized compound

The average thermal stabilities of different mesogenic homologous series are compared and recorded in Table 3.7

Table 3.7: Average thermal stabilities (°C) of Series-I, A and B compounds.

Series	I	A	B
N-Iso	283.73 (C_1-C_{10}, C_{12},C_{14},C_{16})	126.38 (C_2,C_4-C_8, C_{10},C_{12},C_{14},C_{16})	144.62 (C_3-C_8, C_{10},C_{12},C_{14},C_{16},C_{18})
Cr-N	271.13 (C_6-C_8)	107.37 (C_6-C_8)	98.11 (C_3-C_8)

A homologous series of compounds **6a-6m** contains 4-n-decyloxyaniline moiety linked with 4-formylphenyl-7-n-alkoxycoumarin-3-carboxylates forming an azomethine linkage. Series A (Figure 3.22) possesses chalcone linkage at the core of the moiety by which there is an enhancement in the breadth of the compound affecting the linearity and hence responsible for lowering the Cr-N thermal stability of compounds as compared to the **6a-6m** series [68].

In series B (Figure 3.22), coumarin moiety with an alkoxy group at the terminal end is directly linked with azomethine group whereas in Seies-I, coumarin moiety is linked with an ester and a phenyl ring. Hence the absence of ester and a phenyl ring at the core position of the coumarin moiety in series B gets affected resulting in the lowering of Cr-N thermal stability of the compounds.

3.3.9 Antibacterial activity

Table 3.8 below provides an overview of the compounds' in vitro antibacterial activity against *Escherichia coli* (gram –ve) and *Staphylococcus aureus* (gram +ve) Under sterile conditions, sterile nutrient agar plates with about 30 mL of nutrient agar (luria agar) and sterile nutrient broth (soft neutral agar) tubes with 5 mL of nutrient broth are made. A few hours before the experiment, the bacteria were cultivated in the nutritional broth while immersed. The nutrient agar plate is uniformly infected with approximately 0.1 mL of this culture media after the wells have been set and drilled with a sterile cork borer. A dimethyl sulfoxide solution of 10 mg/0.1 mL was produced, and 0.1 mL of this solution was pipetted into each well.

Table 3.8: Antibacterial activity data of compounds (6a-6m) [Series-I]

Compound code	$-C_nH_{2n+1}$, n = no. of carbon atoms in coumarin derivatives	*Escherichia Coli* (zone in mm)	*Staphylococcus aureus* (zone in mm)
6a	1	14.3	16.3
6b	2	14.2	15.8
6c	3	15.2	15.5
6d	4	15.0	16.1
6e	5	14.7	15.6
6f	6	15.7	18.0
6g	7	14.0	16.6
6h	8	15.5	16.7
6i	9	14.6	15.7
6j	10	15.1	18.8
6k	12	14.8	19.0
6l	14	16.0	20.0
6m	16	14.1	18.2
Standard (Streptomycin)		16.0	19.6

The gram-positive bacteria used was *Staphylococcus aureus* while the gram-negative bacteria used was *Escherichia Coli.*

From the anti-bacterial activity data, it was concluded that all the compounds show antibacterial activity against *E. Coli* and *Staphylococcus aureus* as compared to reference standard streptomycin. Amongst all compounds, **6l** shows high antibacterial activity against *E. Coli*, and *Staphylococcus aureus.*

3.4. References

[1] Zhuang ZP, Kung MP, Hou C, Skovronsky DM, Gur TL, Plossl K, Trojanowski JQ, Lee VY, Kung HF. Radioiodinated styrylbenzenes and thioflavins as probes for amyloid aggregates. J. Med. Chem. 2001; **44**(12):1905–1914.

[2] Sreedhar R, Gadhinglajkar SV. Pharmacological neuroprotection. Indian J Anaesth. 2003; **47**(1):8–22.

[3] Bachir M, Riffaud JP, Lacolle JY, Lemoine J, De Almeida A, Houziaux P, Danree B. Synthesis and anticonvulsant activity of some 2-(N-substituted glycylamino)-4-methyl thiazoles. Eur. J. Med. Chem. 1990; **25**(1):71–74.

[4] Najar IA, Kankala RK, Johri RK. Targeted cancer therapies: an overview. Int. J. Life Sci. 2012; **6**(2):61–73.

[5] Rosenzweig KE, Gomez JE. Concurrent Chemotherapy and Radiation Therapy for Inoperable Locally Advanced Non–Small-Cell Lung Cancer. J. Clin. Oncol. 2016; **35**(1):6–10.

[6] Prashanth T, Thirusangu P, Avin BRV, Ranganatha VL, Prabhakar BT, Khanum SA. Synthesis and evaluation of novel benzophenone-thiazole derivatives as potent VEGF-A inhibitors. Eur. J. Med. Chem. 2014; **87**(1):274–283.

[7] Thakur A, Singla R, Jaitak V. Coumarins as anticancer agents: A review on synthetic strategies, mechanism of action and SAR studies. Eur. J. Med. Chem. 2015; **101**(2):476–495.

[8] Sivakumar KK, Rajasekaran A, Ponnilavarasan I, Somasundaram A, Sivasakthi R, Kamalaveni S. Synthesis and evaluation of anti-microbial and analgesic activity of some (4Z)-3-methyl-1-[(2-oxo-2H-chromen-4-yl) carbonyl]-1H-pyrazole-4, 5-dione-4-[(4-substitutedphenyl) hydrazone]. Der Pharm. Lett. 2010; **2**(1):211–219.

[9] Wan Zullkiplee WSH, Mohd Ariff MA, Hussain H, Khairul WM, Ngaini Z. Bacteriostatic activities of N-substituted tris-thioureas bearing amino acid and aniline substituents. Phosphorus. Sulfur. Silicon Relat. Elem. 2016; **191**(10):1329–1333.

[10] Patel RM, Sharma RN, Patel NJ. In vitro cytotoxic screening of 4-methyl-2H-chromen-2-one derivatives against Hep2 cell line. Asian J. Biochem. Pharm. Res. 2011; **1**(2):602–611.

[11] Areti S, Hinge VK, Rao CP. Pyrenyl-imino-C2-glucosyl conjugate: synthesis, characterization, and ratiometric and reversible OFF–ON receptor for Hg+2. Carbohydr. Res. 2014; 399:64–69.

[12] Sandhu S, Bansal Y, Silakari O, Bansal G. Coumarin hybrids as novel therapeutic agents, Bioorg. Med. Chem. 2014; **22**(15):3806–3814.

[13] Goodbye JW, Collings JP, Kato T, Tschierske C, Gleeson H, Raynes P, Vill V, editors. Handbook of Liquid Crystals. 2nd ed., Wiley-VCH, Weinheim, 2014.

[14] Geelhaar T, Griesar K, Reckmann B. 125 years of liquid crystals - a scientific revolution in the home. Angew. Chem. Int. Ed. 2013; **52**(34):8798–8809.

[15] Kato T, Uchida J, Ichikawa T, Sakamoto T. Functional liquid crystals towards the next generation of materials. Angew. Chem. Int. Ed. 2018; 57(1):4355–4371.

[16] Bisoyi HK, Li Q. Liquid crystals: versatile self-organized smart soft materials, Chem. Rev. 2022; **122**(5):912-926.

[17] Wang YF, Shi JW, Chen JH, Zhu WG, Baranoff E. Recent progress in luminescent liquid crystal materials: design, properties and application for linearly polarised emission. J. Mater. Chem. C 2015; **3**(31):7993–8005.

[18] Valeur B, Berberan-Santos M. Molecular Fluorescence: Principles and Applications, 2nd ed., John Wiley & Sons, Weinheim, 2012.

[19] Saccone M, Blanke M, Daniliuc CG, Rekola H, Stelzer J, Priimagi A, Voskuhl J, Giese M. Mesogens with aggregation-induced emission formed by hydrogen bonding. ACS Mater. Lett. 2019; **1**(5):589–593.

[20] Voskuhl J, Giese M. Mesogens with aggregation-induced emission properties: materials with a bright future. Aggregate 2022; **3**(1):121-124.

[21] Wan JH, Mao LY, Li YB, Li ZF, Qiu HY, Wang C, Lai GQ. Self-assembly of novel fluorescent silole derivatives into different supramolecular aggregates: fibre, liquid crystal and monolayer. Soft Matter 2010; **6**(14):3195–3210.

[22] Jian J, Hong F, Xia Z, Zhu D, Liu J, Wu H, Bu X, Cui M, Zeng Z, Wang H. New fluorescent N-heterocyclic liquid crystals with high birefringence. J. Mol. Liq. 2016; **224**(2):909–913.

[23] Grabchev I, Moneva I, Bojinov V, Guittonneau S. Synthesis and properties of fluorescent 1,8-naphthalimide dyes for application in liquid crystal displays. J. Mater. Chem. 2000; **10**(6):1291–1296.

[24] Peng ZH. Synthesis and physical performance of indole and benzimidazole cyanine dyes. J. Mater. Chem. 1996; **6**(4):559–565.

[25] Sims MT. Dyes as guests in ordered systems: current understanding and future directions. Liq. Cryst. 2016; **43**(13-15):2363–2374.

[26] Sung HH, Lin HC. Effect of polar substituents on the properties of 1,3,4-oxadiazole-based liquid crystalline materials containing asymmetric cores. Liq. Cryst. 2004; **31**(6):831–840.

[27] Da Silva FN, Da Silva AS, Bechtold IH, Zapp E, Vieira AA. Luminescent liquid crystals based on 2,1,3-benzoxadiazole: conducive heterocycle or poor cousin of benzothiadiazole. Liq. Cryst. 2019; **46**(9):1707–1717.

[28] Sakurai T, Kobayashi M, Yoshida H, Shimizu M. Remarkable increase of fluorescence quantum efficiency by cyano substitution on an ESIPT molecule 2-(2-hydroxyphenyl) benzothiazole: a highly photoluminescent liquid crystal dopant. Crystals. 2021; **11**(9):1105-1115.

[29] Han J, Wang X, Chang XY, et al. Fluorescent liquid crystalline compounds with 1,3,4-oxadiazole and benzo[b]thiophene units. Liq. Cryst. 2012; **39**(47):669–674.

[30] Arakawa Y, Sasaki S, Igawa K, Tokita M, Konichi G, Tsuji H. Birefringence and photoluminescence properties of diphenylacetylene-based liquid crystal dimers. New J. Chem. 2020; **44**(40):17531–17541.

[31] Guo HY, Yu Q, Xiong YZ, Yang FF. Room-temperature AIE ionic liquid crystals based on diphenylacrylonitrile-imidazole salts. Soft Matter 2020; **16**(45):10368–10376.

[32] Gallardo H, Conte G, Tuzimoto PA, Behramand B, Molin F, Eccher J, Bechtold IH. New luminescent liquid crystals based on 2,1,3-benzothiadiazole and bent five-membered N-heterocyclic cores. Liq. Cryst. 2012; **39**(9):1099–1111.

[33] Buchs J, Gebner A, Heyne B, Janietz D, Sawade H. Fluorescent liquid crystals with rod-shaped π-conjugated hydrocarbon core. Liq. Cryst. 2019; **46**(2):281–298.

[34] Karim MR, Sheikh MRK, Yahya R, Salleh NM, Azzahari AD, Hassan A, Sarih NM. Thermal, optical and electrochemical study of side chain liquid crystalline polymers bearing azo-benzothiazole chromophore in the mesogen. J. Polym. Res. 2013; **20**(10):251-259.

[35] Yang ZW, Huang XY, Cheng JC, Guo HG, Yang FF. Novel fluorescence liquid crystals based on thiophene-vinylnitrile Schiff-base derivatives. Liq. Cryst. 2022; **12**(1):24-34.

[36] Paul MK, Singh YD, Dey A, Saha SK, Anwar S, Chattopadhyay AP. Coumarin based emissive rod shaped new schiff base mesogens and their zinc (II) complexes: synthesis, photophysical, mesomorphism, gelation and DFT Studies. Liq. Cryst. 2016; **43**(2):343–360.

[37] Zhang H, Liu XC, Gong YX, Yu TZ, Zhao YL. Synthesis and characterization of SFX-based coumarin derivatives for OLEDs, Dyes Pigment. 2021; **185**(1):108969.

[38] Zhang H, Luo QL, Mao YZ, Zhao YL, Yu TZ. Synthesis and characterization of coumarin-biphenyl derivatives as organic luminescent materials, J. Photochem. Photobiol. A 2017; **346**(4):10–16.

[39] Merlo AA, Tavares A, Khan S, Leite Santos MJ, Teixeira SR. Liquid-crystalline coumarin derivatives: contribution to the tailoring of metal-free sensitizers for solar cells. Liq. Cryst. 2018; **45**(2):310–322.

[40] Mohammad AKT, Mustafa HK. Unsymmetrical coumarin based dimeric liquid crystals: synthesis, characterization, mesomorphic investigation, photoluminescence and thermal conductivity. Liq. Cryst. 2022; **49(**14):354–365.

[41] Seed A. Synthesis of self-organizing mesogenic materials containing a sulfur-based five-membered heterocyclic core. Chem. Soc. Rev. 2007; **36**(12):2046–2069.

[42] Andrienko D. Introduction to liquid crystals. J. Mol. Liq. 2018; **267**(2):520-541.

[43] Matharu AS, Jeeva S, Ramanujam P. Liquid crystals for holographic optical data storage. Chem. Soc. Rev. 2007; **36**(12):1868–1880.

[44] Lagerwall JPF, Scalia GA. New era of liquid crystal research: applications of liquid crystals in soft matter nano-, bio- and microtechnology. Curr. Appl. Phy. 2012; **12**(6): 1387-1412.

[45] Han J. 1,3,4-Oxadiazole based liquid crystals. J. Mater. Chem. C. 2013; **1**(47):7779-7797.

[46] Aldred MP, Vlachos P, Dong D, Kitney SP, Tsoi WS, Neill MO, Kelly SM. Heterocyclic reactive mesogens: synthesis, characterisation and mesomorphic behaviour. Liq. Cryst. 2005; **32**(8):951–965.

[47] Craig AA, Imrie CT. Effect of spacer length on the thermal properties of side-chain liquid crystal polymethacrylates. 2. Synthesis and characterization of the poly [omega-(4′-cyanobiphenyl-4-yloxy) alkyl]methacrylates. Macromol. 1995; **28**(10):3617–3624.

[48] Henderson PA, Seddon JM, Imrie CT. Methylene- and ether- linked liquid crystal dimers II. Effects of mesogenic linking unit and terminal chain length. Liq Cryst. 2005; **32**(12):1499–1513.

[49] Saad GR, Ahmed NHS, Fahmi AA, et al. Influence of lateral methyl and terminal substituents on the mesophase behaviour of four rings azo-ester liquid crystal compounds. Liq Cryst. 2019; **46**(77):1285–1297.

[50] Ge LN, Xian SW, Huang Y, et al. Synthesis and mesomorphism of novel multi-arm liquid crystals with cholic acid as chiral centre linking Schiff base moieties as mesogens. Liq Cryst. 2017; **45**(2):1055–1067.

[51] Yeap GY, Osman F, Imrie CT. Non-symmetric chiral liquid crystal dimers. Preparation and characterization of the (S)-(benzylidene-4′-substitutedaniline)-2″-methylbutyl-4‴-(4‴″-phenyloxy)-benzoateoxy) hexanoates. J. Mol Stru. 2016; **1111**(2):118–125.

[52] Hagar ME, Ahmed HA, Saad GR. Synthesis and mesophase behaviour of Schiff base/ester 4-(arylideneamino)phenyl-4”-alkoxy benzoates and their binary mixtures. J Mol Liq. 2019; **273**(5):266–273.

[53] Ahmed HA, Hagar ME, Saad GR. Impact of the proportionate of dialkoxy chain length on the mesophase behavior of Schiff base/ester liquid crystals; experimental and theoretical study. Liq Cryst. 2019; **23**(7):1–10.

[54] Ahmed HA, Hagar M, El-Sayed TH, et al. Schiff base/ester liquid crystals with different lateral substituents: mesophase behaviour and DFT calculations. Liq Cryst. 2019; **24**(8):1–11.

[55] Hagar M, Ahmed HA, Saad GR. Mesophase stability of new Schiff base ester liquid crystals with different polar substituents. Liq Cryst. 2018; **45**(12):1324–1332.

[56] Yeap G-Y, Mohammad AKT, Osman H. Synthesis and anisotropic properties of novel asymmetric diones fused with 1,3-oxazepine and oxazepane rings. Mol Cryst LiqCryst. 2012; **552**(1):177–193.

[57] Mohammad AKT, Srinivasa HT, Tiong HS, et al. Synthesis and comparative studies of phase transition behaviour of new dimeric liquid crystals consisting of dimethyluracil and biphenyl cores. J Mol Liq. 2016; **219**:765–772.

[58] Mohammad AKT, Srinivasa HT, Mohammed HM, et al. Synthesis mesomorphic and theoretical studies of some new unsymmetrical dimeric ethers of 6-amino-1,3- dimethyluracil and biphenyl cores. J Mol Struct. 2016; **1117**:201–207.

[59] Mohammad AKT, Srinivasa HT, Hariprasad S, et al. Enhanced liquid crystal properties in symmetric ethers containing the oxazepine core: synthesis and characterization of seven member heterocyclic dimers. Tetrahedron. 2016; **72**(1):3948–3957.

[60] Mohammad AKT, Srinivasa HT, Hariprasad S, et al. New mesogenic compounds possessing abiphenyl ester and ether moiety comprising 1,3-dimethylbarbituric acid: synthesis: characterisation and mesomorphic studies. Liq Cryst. 2016; **43**(9):1174–1183.

[61] Paul MK, Singh YD, Dey A, et al. Coumarin based emissive rod shaped new schiff base mesogens and their zinc(II) complexes: synthesis, photophysical, mesomorphism, gelation and DFT studies. Liquid Crystals. 2016; **43**(10):343–360.

[62] He J, Zhao Y, Zhao Y. Photoinduced bending of a coumarin-containing supramolecular polymer. Soft Matter. 2009; **5**(2):308–310.

[63] Li Y, Chen X, Chen P, et al. Synthesis and mesomorphic properties of 7-alkoxybezopyrano[2,3-c]pyrazol-3-one. Liquid Crystals. 2010; **37**(2):1549–1557.

[64] Annunziata F, Pinna C, Dallavalle S, et al. An overview of coumarin as a versatile and readily accessible scaffold with broad-ranging biological activities. International Journal of Molecular Sciences. 2020; **21**(1):1–83.

[65] Stefanachi A, Leonetti F, Pisani L, et al. Coumarin: A natural, privileged and versatile scaffold for bioactive compounds. Molecules. 2018; **23**(2): 250-270.

[66] Hoult JRS, Payá M. Pharmacological and biochemical actions of simple coumarins: Natural products with therapeutic potential. General Pharmacology. 1996; **27**(1):713–722.

[67] Stepanenko I, Babak M V., Spengler G, et al. Coumarin-based triapine derivatives and their copper(II) complexes: Synthesis, cytotoxicity and mr2 rnr inhibition activity. Biomolecules. 2021; **11**(6):1–21.

[68] Durgapal SD, Soni R, Soman SS, et al. Synthesis and mesomorphic properties of coumarin derivatives with chalcone and imine linkages. Journal of Molecular Liquids [Internet]. 2020; **297**:111920.

[69] Abdel-Wahab BF, Mohamed HA, Farhat AA. Ethyl coumarin-3-carboxylate: Synthesis and chemical properties. Organic Communications. 2014; **7**(1):1–27.

[70] Trivedi KN, Thaker NN. MESOMORPHIC HETEROCYCLIC HOMOLOGOUS SERIES: I. 7-(4' -n-ALKOXYBENZOYLOXY)-3-ACETYLCOUMARINS II. 4' -FORMYLPHENYL 7-n-ALKOXYCOUMARIN-3-CARBOXYLATES. Molecular crystals and liquid crystals. 1981; **78**:263–270.

[71] Molecular Crystals and Liquid Crystals Alkyl Carbonato Terminally Substituted Anils. 2007; **22**(3-4):37–41.

[72] Jain V, Kaur S, Mohiuddin G, et al. Design, Synthesis and Characterization of Achiral Unsymmetrical Four-ring based Hockey-stick Shaped Liquid Crystals: Structure-Property relationship. Liquid Crystals. 2022; **49**(7-9):162–171.

[73] Tomi IHR, Al-Karawi AJM, OmarAli AAB, et al. Liquid crystal behavior of Ag(I) complexes based on a series of mesogenic 1,3,4-thiadiazole ligands. Molecular Crystals and Liquid Crystals [Internet]. 2021; **722**(1):8–26.

[74] Donaldson T, Staesche H, Lu ZB, et al. Symmetric and non-symmetric chiral liquid crystal dimers. Liquid Crystals. 2010; **37**(8):1097–1110.

[75] Yeap GY, Lee HC, Mahmood WAK, et al. Synthesis, thermal and optical behaviour of non-symmetric liquid crystal dimers -(4-benzylidene-substituted-aniline-4′-oxy) - [pentyl-4-(4′- phenyl)benzoateoxy]hexane. Phase Transitions. 2011; **84**(1):29–37.

[76] Chan TN, Lu Z, Yam WS, et al. Non-symmetric liquid crystal dimers containing an isoflavone moiety. Liquid Crystals. 2012; **39**(1):393–402.

[77] Satheeshkumar R, Sayin K, Kaminsky W, et al. Synthesis, spectral analysis and quantum chemical studies on molecular geometry, chemical reactivity of 7-chloro-9-(2′-chlorophenyl)-2,3-dihydroacridin-4(1H)-one and 7-chloro-9-(2′-fluorophenyl)-2,3-dihydroacridin-4(1H)-one. Journal of Molecular Structure. 2017; **1128**:279–289.

[78] Khushaim MS, Alalawy HH, Naoum MM, et al. Experimental and computational simulations of nematogenic liquid crystals based on cinnamic acid in pure and mixed state. Liquid Crystals. 2021; **48**(1):1493–1504.

[79] Sharma D, Tiwari SN. Comparative computational analysis of electronic structure, MEP surface and vibrational assignments of a nematic liquid crystal: 4-n-methyl-4’-cyanobiphenyl. Journal of Molecular Liquids. 2016; **214**(1):128–135.

[80] Walker R, Pociecha D, Strachan GJ, et al. Molecular curvature, specific intermolecular interactions and the twist-bend nematic phase: the synthesis and characterisation of the 1-(4-

cyanobiphenyl-4′-yl)-6-(4-alkylanilinebenzylidene-4′-oxy)hexanes (CB6O.m). Soft Matter. 2019; **15**:3188–3197.

[81] Petrov VF. Alkoxylation in achiral calamitic liquid crystals. Liquid Crystals. 2002; **29**(6):805–835.

[82] Walker R, Pociecha D, Storey JMD, et al. Remarkable smectic phase behaviour in odd-membered liquid crystal dimers: The CT6O.m series. Journal of Materials Chemistry C. 2021; **9**(15):5167–5173.

[83] Paskin A. Physical review letters 1890; **33**(2):300–303.

[84] De Jeu WH, van der Veen J. Molecular Structure and Nematic Liquid Crystalline Behaviour. Mol Cryst Liq Cryst. 1976; **40**(4):1–17.

[85] Date RW, Imrie CT, Luckhurst GR, et al. Smectogenic dimeric liquid crystals: The preparation and properties of the α,ω-bis(4-n-alkylanilinebenzylidine-4′-oxy)alkanes. Liquid Crystals. 1992; **12**(1):203–238.